NPEPPS regulates intracellular import and sensitivity to cisplatin by interaction with volume-regulated anion channels

Robert T. Jones[1,13], Andrew Goodspeed[1,2,13], Saswat Mohapatra[3], Lily Elizabeth Feldman[1], Mathijs Scholtes[4], Hedvig Vekony[1], Annie Jean[1], Charlene B. Tilton[1], Michael V. Orman[1], Cailin Deiter[1], Nathaniel Xander[1], Stephanie Araki[1], Molishree Joshi[1,5], Mahmood Javaid[6], Eric T. Clambey[7], Ryan Layer[6,8], Teemu D. Laajala[1,9], Sarah Parker[10], Tahlita Zuiverloon[4,*], Dan Theodorescu[3,11,12,*], and James C. Costello[1,2,14,*]

[1]Department of Pharmacology, University of Colorado Anschutz Medical Campus, Aurora, CO, USA
[2]University of Colorado Cancer Center, University of Colorado Anschutz Medical Campus, Aurora, CO, USA
[3]Cedars-Sinai Samuel Oschin Comprehensive Cancer Institute, Los Angeles, CA, USA
[4]Department of Urology, Erasmus MC Cancer Institute, Erasmus University Medical Center Rotterdam, Rotterdam, The Netherlands
[5]Functional Genomics Facility, University of Colorado Anschutz Medical Campus, Aurora, CO, USA
[6]Computer Science Department, University of Colorado, Boulder
[7]Department of Anesthesiology, University of Colorado Anschutz Medical Campus, Aurora, CO
[8]BioFrontiers Institute, University of Colorado, Boulder
[9]Department of Mathematics and Statistics, University of Turku, Turku, Finland.
[10]Smidt Heart Institute & Advanced Clinical Biosystems Research Institute, Cedars Sinai Medical Center, Los Angeles, California 90048, United States
[11]Department of Surgery, Cedars-Sinai Medical Center, Los Angeles, CA, USA
[12]Department of Pathology and Laboratory Medicine, Cedars-Sinai Medical Center, Los Angeles, CA, USA
[13]Equal first authors
[14]Lead Contact
*Corresponding Authors

Corresponding Authors

Tahlita Zuiverloon, MD, PhD
Department of Urology
Erasmus MC Cancer Institute, Erasmus University Medical Center
Dr. Molewaterplein 40, 3015GD, Rotterdam
The Netherlands
+31 6 26 41 90 87
t.zuiverloon@erasmusmc.nl

Dan Theodorescu, MD, PhD
Departments of Surgery and Pathology
Cedars-Sinai Medical Center
8700 Beverly Blvd. OCC Mezz C2002
10/2/22 2:31:00 PMLos Angeles, CA 90048
+1 (310) 423-8431
dan.theodorescu@cshs.org

James C Costello, PhD
Department of Pharmacology
University of Colorado Anschutz Medical Campus
Mail Stop 8303
12801 E. 17th Ave., Rm L18-6114
Aurora, CO 80045
+1 (303) 724-8619
james.costello@cuanschutz.edu

KEY WORDS

NPEPPS; Volume Regulated Anion Channel; CRISPR Screen; Synthetic Lethality; multi-omics; Bladder Cancer; DNA Repair; Cisplatin; Chemoresistance

ABSTRACT

Despite routine platinum-based chemotherapeutic use in cancer treatment, there remains a need to improve efficacy and patient selection. Using multi-omic assessment of cisplatin responsive and resistant human bladder cancer cell lines and whole-genome CRISPR screens, we identified NPEPPS, the puromycin-sensitive aminopeptidase as a novel driver of cisplatin resistance. Volume-regulated anion channels (VRACs) have been shown to directly import the majority of intracellular cisplatin. Here, we show that the mechanism of NPEPPS-mediated cisplatin resistance is by binding to VRACs and blocking the import of cisplatin into the cell. We show that NPEPPS depletion increased intracellular cisplatin and made cisplatin-resistant cells more responsive to cisplatin *in vitro* and *in vivo*. Overexpression of NPEPPS in cisplatin-sensitive cells decreased intracellular cisplatin and resulted in increased treatment resistance. The same results also hold for carboplatin. Our findings describe the first mechanism by which VRACs can be targeted to control the import of cisplatin and carboplatin.

INTRODUCTION

Platinum-based chemotherapeutics have a long history[1,2] with successful applications in testicular, ovarian, bladder, head and neck, and lung cancers. However, these drugs come with dose-dependent side effects that limit patient eligibility. Additionally, chemoresistance mechanisms can arise, reducing the efficacy of these drugs. While mechanisms of resistance have long been established, including DNA damage repair and drug export[3], other mechanisms, such as the import of platinum-based drugs through volume regulated anion channels (VRACs) are more recently discovered and present new opportunities for therapeutic development[2,4]. However, there is no known mechanism by which VRAC activity can be targeted to control the import of platinum drugs.

Despite the limitations of platinum-based drugs, they remain the standard of care in many cancer types and with a paucity of better treatment options for many patients, these drugs will remain in use for the foreseeable future. Two avenues can improve patient outcomes, which include the discovery of more effective agents or the development of strategies that can improve the efficacy of platinum-based regimens. The latter would have a broad impact across a range of cancer types. Here we take the latter approach and focus our efforts on bladder cancer.

Bladder cancer (BCa) accounts for 430,000 new diagnoses and 170,000 deaths worldwide annually[5]. Cisplatin-based combination chemotherapy, in the form of gemcitabine plus cisplatin (GemCis) or Methotrexate, Vinblastine, Adriamycin, and Cisplatin (MVAC), remains the first-line, standard of care for metastatic BCa, providing a 5-10% cure rate. However, up to 30% of patients are ineligible for cisplatin-based treatment[6] and are offered carboplatin-based combinations. Unfortunately, carboplatin combination therapy has been shown to be less effective in BCa[7]. Alternatively, immune checkpoint therapies (ICT) are being used as a first-line therapy[8]; however, ICT requires a PD-L1 diagnostic test, for which only ~25% patients meet eligibility[9]. On top of limited patient eligibility, the complete response rates for ICT eligible patients is 20-30%[10], which limits the overall efficacy of ICT across the population of patients with metastatic BCa. Cisplatin-based combination chemotherapy is also standard of care in the neoadjuvant (NAC) setting for the management of localized muscle-invasive bladder cancer[11,12]. However, NAC adoption has been slow due to the toxicity of the drugs, the number of patients that are ineligible for cisplatin, and the relatively small survival benefit of 5-15% over immediate cystectomy[13]. Importantly, in both the metastatic and NAC BCa settings, patient selection and therapeutic efficacy of cisplatin-based chemotherapy remain critical unresolved challenges[7].

Recently, several large-scale efforts have performed whole genome loss-of-function screening across hundreds of cancer cell lines using CRISPR- and shRNA-based libraries to define pan-cancer and context-specific genetic dependencies[14–17]. While these efforts have been critical in defining genetic dependencies in cancer, a limitation is that cells were grown under basal growth conditions in the absence of any treatment. Additionally, those studies were performed in cell lines that had not acquired resistance to any treatments. To better understand the functional drivers of therapeutic resistance, such screens must be done in the presence and absence of the therapy of interest[18–21], and in cells that have acquired resistance to the treatment itself. Results from such synthetic lethal screens can be used to prioritize gene candidates that can be targeted to overcome or prevent treatment resistance.

In this study, we harnessed the power of CRISPR-based synthetic lethal screening and multi-omic profiling to systematically assess the functional determinants of sensitivity to the treatment regimen of gemcitabine plus cisplatin in a panel of chemoresistant BCa cell lines (**Figure 1A**). In addition to known mechanisms, we present the finding that puromycin-sensitive

129 aminopeptidase, NPEPPS, is a novel mechanism of cisplatin resistance with *in vitro* and *in vivo*
130 validation. We determine that the mechanism of NPEPPS-mediated resistance is by directly
131 controlling the import of cisplatin via interaction with VRACs. These findings describe the first
132 mechanism by which VRAC function can be targeted for therapeutic benefit. We finally provide
133 a unique resource to the community, an R Shiny app for broad comparisons between datasets
134 (CRISPR screens and multi-omic) and cell lines, along with individual gene queries and basic
135 plotting functionality (https://bioinformatics.cuanschutz.edu/BLCA_GC_Omics/).

RESULTS

From the Resistant Cancer Cell Line (RCCL) collection[22,23], we acquired the five human BCa cell lines, KU1919, 5637, T24, TCCSUP, and 253J. For each, we obtained the parental lines (-Par) and their matched derivatives that were made resistant through dose escalation to cisplatin (-Cis), gemcitabine (-Gem), and the combination of gemcitabine plus cisplatin (-GemCis) (**Figure 1A; Table S1**). We confirmed resistance to the associated drugs for all resistant derivatives in comparison to the parental lines and found them to be consistent with those reported by the RCCL (**Figure S1**)[22,23]. These cells represent features and alterations in putative BCa drivers as reported in TCGA[24] and variants reported in ClinVar[25] (**Tables 1**, **S2** and **S3)**.

Genome-wide CRISPR screens identify 46 common synthetic lethal genes

To study the connection between drug resistance and gene expression, we performed whole-genome loss-of-function screens in each of the five GemCis-resistant cell line derivatives. After transduction of the Brunello CRISPR-Cas9 knockout library[26], we passaged the cells for 10 days to clear essential genes, then split them into saline (PBS) or gemcitabine plus cisplatin treatment groups (**Figure 1A**). Each screen was performed at a drug concentration that allowed the GemCis-resistant cells to grow unrestricted, but which significantly inhibited the growth of the associated parental lines (**Table S1**). Screening parameters for each cell line are reported in **Table S4**. We counted sgRNAs 19 and 25 days after transduction, which were 9 and 15 days after the start of treatment. Patterns of correlation between treatment conditions and cell lines were consistent, and as expected grouped by experimental conditions (**Figure S2**).

We defined genes as “synthetic lethal” with gemcitabine plus cisplatin treatment as those for which the combined cognate sgRNA counts were significantly lower (moderated t-test, FDR < 0.05) in the gemcitabine plus cisplatin-treated arm compared to the PBS arm when including both days 19 and 25 in the statistical model (**Table S5**). We identified 235 synthetic lethal genes that were statistically significant in KU1919-GemCis, 888 for T24-GemCis, 2099 for TCCSUP-GemCis, 2369 for 253J-GemCis, and 511 for 5637-GemCis. Next, we performed gene set enrichment analysis[27] on the full ranked list of genes according to their synthetic lethality. For this analysis, we created one ranked gene list by including each of the five cell types in the statistical model directly. As expected, and as a validation of the screen itself, we found that the top-ranked pathways were dominated by processes such as DNA repair, Fanconi Anemia, nucleotide excision repair, double-stranded break repair, base-excision repair, and DNA damage bypass mechanisms (**Figure 1B** and **Table S6**). These results are consistent with the known roles of DNA damage detection and repair in cisplatin resistance[3,28]. Providing additional validation, we cross-referenced our list CRISPR screen results with a set of manually curated genes associated with platinum resistance in cancer[29] and found that the ranked list of hits are enriched for genes known to be associated with platinum resistance (**Table S5**).

Next, we sought to identify the most robust and commonly synthetic lethal candidate genes by identifying only those significant in all 5 cell lines (**Figures 1C** and **S3**). Of the 46 commonly synthetic lethal genes, as illustrated in **Figure 1D**, some increased cell growth in PBS treatment, then reduced growth in gemcitabine plus cisplatin treatment. Other genes had very little impact on cell growth in PBS treatment, but then reduced growth when treated with gemcitabine plus cisplatin. Finally, some genes reduced cell growth in PBS treatment and further reduced growth with gemcitabine plus cisplatin treatment. Of the 46 common synthetic lethal candidate genes, 41 fell into one or more putative DNA damage response and repair pathways, including

homologus recombination, double-stranded break repair, nuclear excision repair, and Fanconi anemia (**Figure S3B** and **Table S7**).

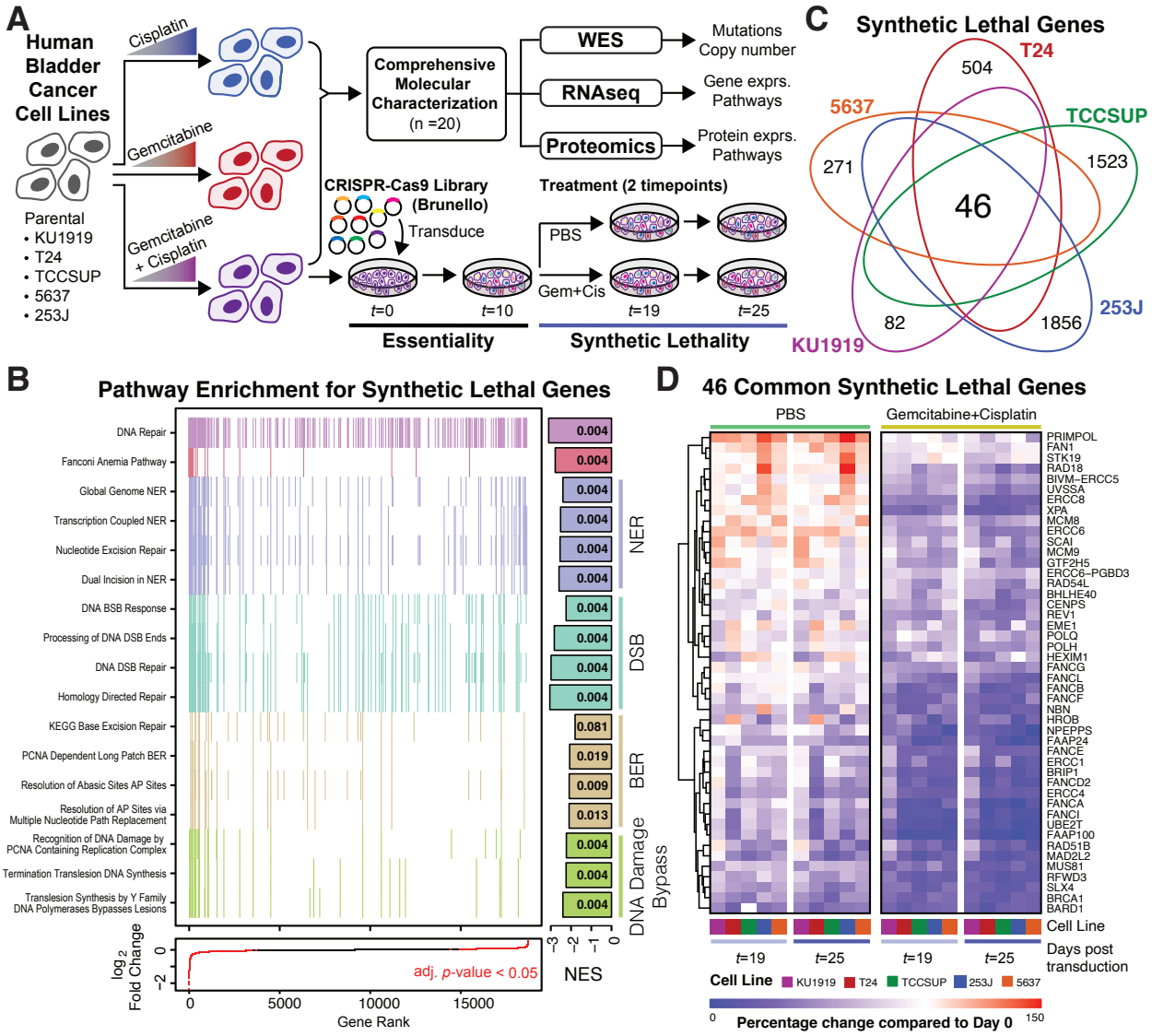

Figure 1. Project overview and synthetic lethal screen results. (**A**) Human bladder cancer cell lines were made resistant to cisplatin, gemcitabine, or gemcitabine plus cisplatin through dose escalation. All cell lines were profiled using -omic technologies. The gemcitabine plus cisplatin-resistant cells were subjected to a pooled CRISPR screen to identify synthetic lethal gene-to-drug relationships. (**B**) Aggregate gene set enrichment results for the synthetic lethal screen ranked by $\log_2$ fold change across all cell lines reveal DNA damage response and repair pathways. Each tick mark represents a gene in the associated pathway. The bars at the right are normalized enrichment scores (NES) with the FDR corrected p-values reported in the bars. (**C**) The intersection across the CRSIPR screen results identified 46 common synthetic lethal genes; all counts and gene annotation are reported in **Figure S2**. (**D**) The percentage change in the aggregate of the sgRNAs targeting the 46 commonly synthetic lethal genes are reported across saline (PBS) or gemcitabine plus cisplatin treatment arms of the CRISPR screen. Cell lines are coded with the same colors throughout all figures.

201

Feature	KU1919	T24	TCCSUP	5637	253J
Sex	Male	Female	Female	Male	Male
Stage	T3	Ta	N/A	N/A	T4
Grade	G3	G3	G4	G2	G4
Base47 Subtype	N/A	Basal	Basal	Luminal	Basal
TP53		Y126X	E349X		
HRAS		G12V			
NRAS	Q61R				
PIK3CA			E545K		E545G
TERT					
ARID1A	Y1052X				
KMT2D	T2441Pfs*44			Q2813X	
KDM6A	Q915X				
FAT1		S2682X	D1536N		
KMT2C		R4225X; A3559T			
ERBB2				S310F	
ERBB3		E1219K			
EP300		C1201Y			
FBXW7			S66X		
ASXL2			E330Q		
ATM				H1876Q	
AKT1	E17K				
RYR2		R2401H			
NFE2L2					G81S
RB1			LOSS	Y325X	
E2F3			AMP	AMP	
PPARG				AMP	
CCND1	AMP				
CDKN2A	LOSS				LOSS

202 **Table 1.** Clinicopathologic characteristics and genetic drivers for five cell lines.

NPEPPS is a novel regulator of response to cisplatin

A recent systematic analysis of hundreds of CRISPR screens in cancer cell lines with comprehensive multi-omic profiling demonstrated that transcript expression markers were the best predictors of gene dependency[30], providing the rationale for the use of pre-treatment -omic profiling as a means to study the biological impact of synthetic lethal hits. Hence, to prioritize the 46 common synthetic lethal genes for validation and detailed mechanistic study, we performed RNA sequencing and mass spectrometry-based proteomic profiling on cell lysates of all cell lines grown in drug-free media (**Figure 1A**).

We investigated the transcriptome and proteome data by comparing parental to matched drug-resistant derivative lines (-Gem, -Cis, and -GemCis) and identified several known mechanisms of chemoresistance. For example, acquired resistance to gemcitabine follows a number of common pathways across multiple tumor types that disrupt intracellular metabolism, such as the loss of deoxycytidine kinase (DCK) or increased expression of ribonucleotide reductase subunit M1 (RRM1)[31–33] (**Figure S4A**). Our data shows that RRM1 is specifically and significantly upregulated in nearly all Gem- and GemCis-resistant derivatives in the T24, TCCSUP, KU1919, and 5637 cell line series by both RNA and protein expression. In addition, and with the TCCSUP-GemCis line being the only exception, we found RRM1 copy number amplified, but not in the parental or the cisplatin-resistant cells, providing strong support that a robust and consistently acquired mechanism of gemcitabine resistance in these cells is the copy number amplification and subsequent upregulation of RRM1 (**Figure S4B**). RRM1 is defined as an essential gene in the Dependency Map[16], which we also detected in our screen (**Table S8**). Interestingly, in 253J-Gem and 253J-GemCis cell lines, which had minor changes in RRM1 expression, DCK expression was lost at the RNA and protein level with these results being supported by a copy number loss specific to these cells (**Figure S4B**).

Next, we analyzed gene and protein expression together while treating the cell line as a covariate in the statistical model. We found 1557 significantly upregulated genes across the Gem-resistant lines, 1897 in the Cis-resistant lines, and 1530 in the GemCis-resistant lines (moderated t-test, FDR < 0.05; **Table S9**). The proteomics data revealed 9 significantly upregulated proteins across the Gem-resistant cell lines, 1 in the Cis-resistant cell lines, and 10 in the GemCis-resistant cell lines (moderated t-test, FDR < 0.25; **Table S10**). Given the lower number of significant proteins and the relevance of transcript expression in predicting genetic dependency[30], we first investigated the overlap between the CRISPR screen results and the transcriptomes from each of the resistant cell line derivatives compared to the parental cells. Few genes were significantly and consistently upregulated across the resistant derivatives in the list of 46 commonly synthetic lethal genes (**Figure 2A**), but the most significantly and consistently upregulated genes were involved in DNA damage response and repair mechanisms, including ERCC6, XPA, REV1, POLH, ERRC8, PRIMPOL, NBN, and members of the Fanconi Anemia pathway. Puromycin-sensitive aminopeptidase, NPEPPS, was identified as being the most consistently upregulated gene across the resistant derivatives (**Figure 2A, B**). We similarly found protein levels to be consistently and significantly upregulated (**Figure 2C**). NPEPPS was also a top synthetic lethal hit (**Figure 2D** and **Table S5**). Consistent with the proteomics results, immunoblotting for NPEPPS revealed that it was upregulated in the Cis-resistant and GemCis-resistant lines, with the Gem-resistant lines showing variable upregulation (**Figure 2E**).

We examined an independent whole-genome CRISPR screen that tested 27 general genotoxic agents[21] and here we report new findings in support of NPEPPS as a novel mediator of cisplatin

253 resistance. We found that cells with NPEPPS loss were specifically depleted in response to
254 cisplatin, but not gemcitabine (**Figure 3A**). This result strongly supports the robustness of our
255 findings as Olivieri et al. used different CRISPR libraries (TKOv2 and TKOv3) and cell line
256 (retinal pigment epithelium-1, RPE1). Moreover, our screen results for all five cell lines were
257 highly correlated with the three cisplatin screens (**Figure S5A**). Strikingly, nearly all 46 common
258 synthetic lethal genes were significantly associated with cisplatin, but not gemcitabine in Olivieri
259 et al. (**Figure S5B**).
260
261 To validate our finding that NPEPPS depletion enhances sensitivity to gemcitabine plus cisplatin
262 treatment in GemCis-resistant BCa cells, and to parse its role in both cisplatin and gemcitabine
263 resistance, we generated stable NPEPPS shRNA knockdowns in the KU1919-GemCis and T24-
264 GemCis cell lines. We found that NPEPPS knockdown preferentially increased cisplatin, but not
265 gemcitabine sensitivity (**Figure 3C, E**). Knockdown of NPEPPS did delay growth of cells but did
266 not have major effects on cell growth rates (**Figure S6A**). siRNA targeting of NPEPPS in the
267 KU1919-GemCis cell line and shRNA and/or siRNA in T24-GemCis and 253J-GemCis cells
268 confirmed our results that NPEPPS loss preferentially sensitizes cells to cisplatin (**Figure**
269 **S6B,C**). Additionally, we used a gRNA from the CRISPR screen library to show both strong
270 knockout of NPEPPS and the associated dose response matching our findings with shRNA and
271 siRNA (**Figure S6D**). To complement these findings, we overexpressed NPEPPS in KU1919
272 and T24 parental lines and found increased treatment resistance to cisplatin, but not
273 gemcitabine (**Figure 3D, F**). We also found NPEPPS mRNA increased with cisplatin
274 concentrations in both KU1919-Par and KU1919-GemCis cells after 24 hours of treatment
275 (**Figure 3B**). These results indicate that NPEPPS responds to cisplatin exposure and mediates
276 sensitivity to gemcitabine plus cisplatin by its effect on resistance to cisplatin.

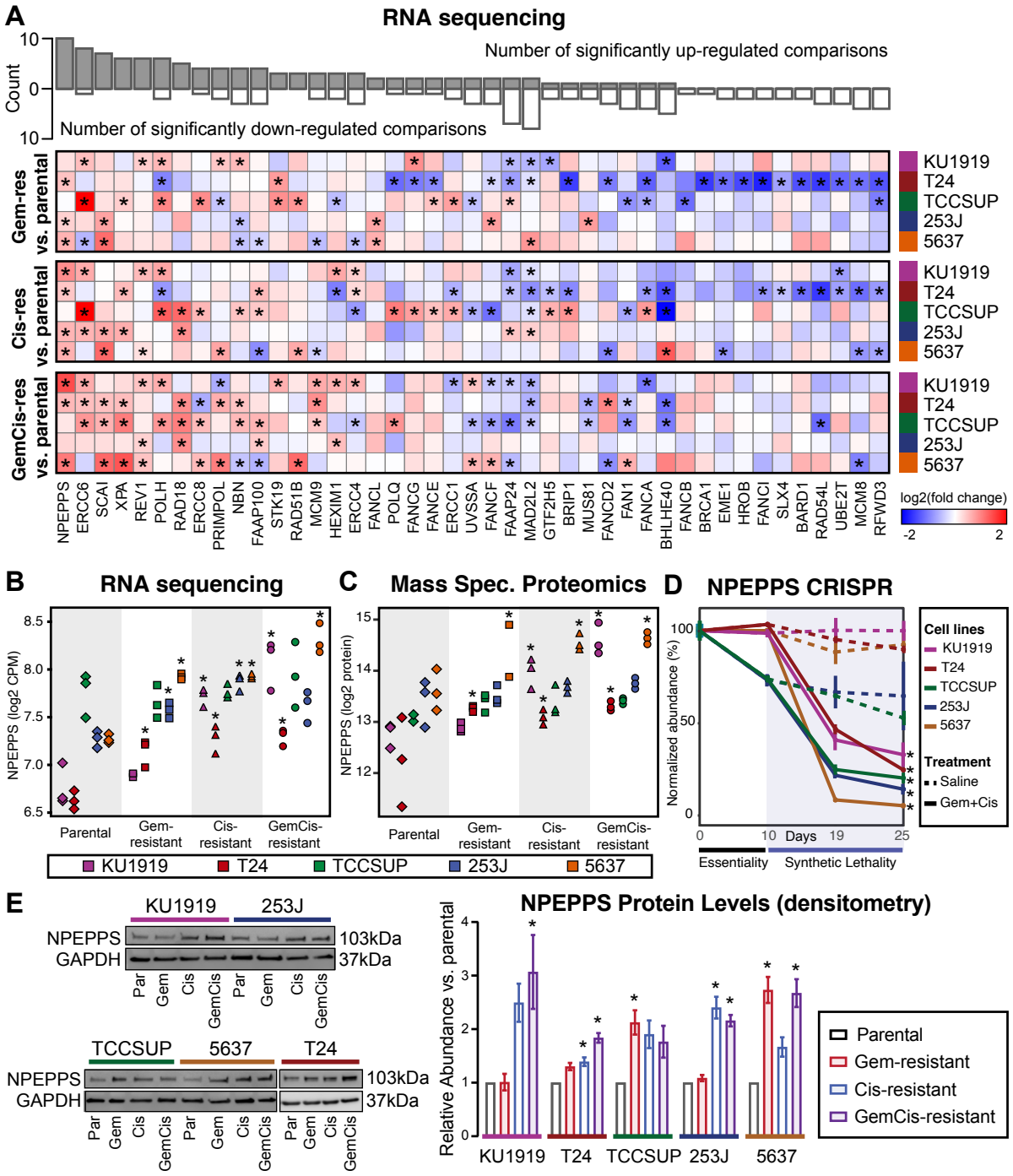

Figure 2. NPEPPS is identified as a commonly upregulated and synthetic lethal hit. (**A**) Differential gene expression of the 46 common synthetic lethal genes as measured by RNAseq across all cell lines, comparing the treatment-resistant derivative (Gem-, Cis-, GemCis-resistant) to the associated parental cell line. Asterisks indicate a statistically significant result (moderated t-test, *FDR < 0.05). The bar plot on top is the aggregate count of significant results across all 15 comparisons. Genes are ranked by the count of statistically significant upregulated hits. (**B**) RNAseq (moderated t-test compared to parentals; *FDR < 0.05), (**C**) mass spectrometry proteomics (moderated t-test compared to parentals, *FDR < 0.25), and (**D**) CRISPR screen results for NPEPPS (mean ± SD; moderated t-test; *FDR < 0.05). (**E**) Representative immunoblots and densitometry quantification for independent triplicates (mean ± SEM) for NPEPPS in all cell lines (*FDR < 0.05).

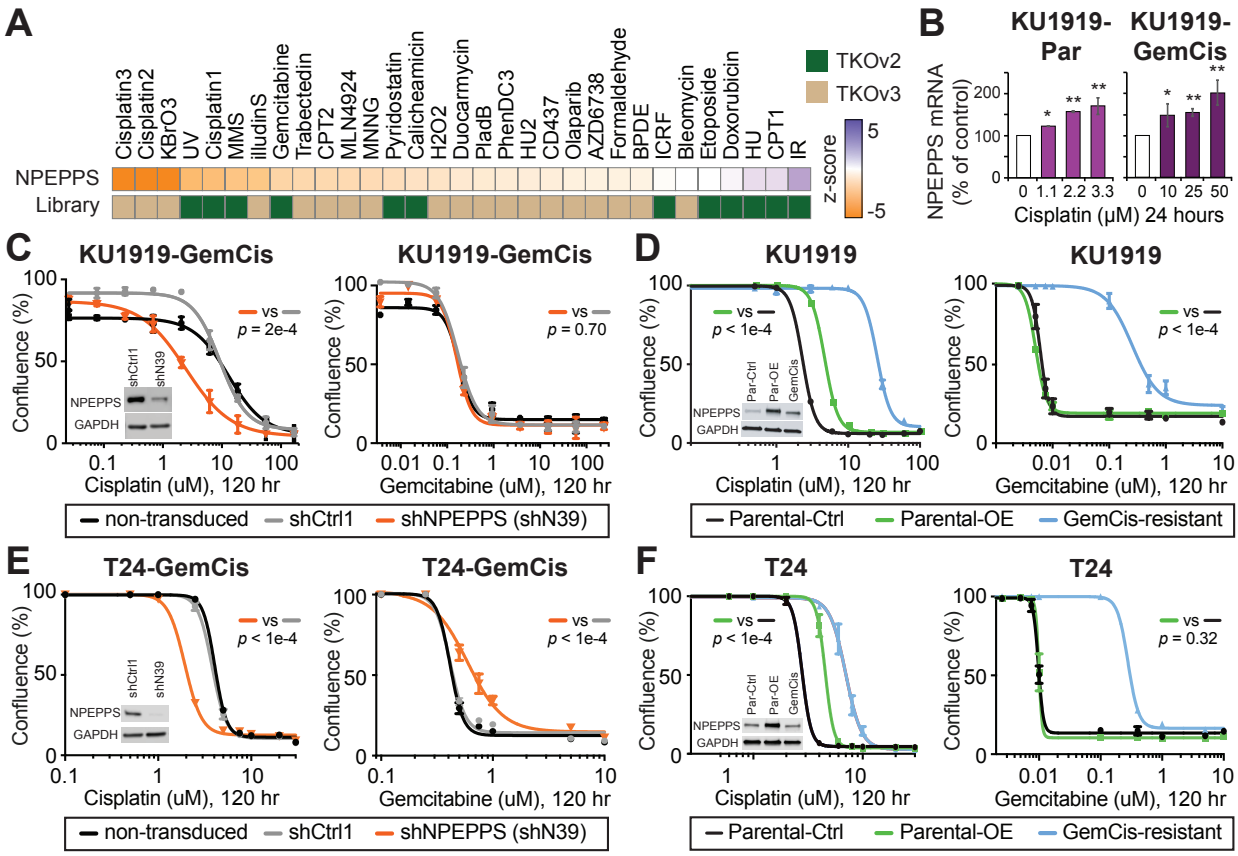

Figure 3. Genetic inhibition of NPEPPS resensitizes GemCis-resistant cells. (**A**) NPEPPS was found to be synthetic lethal with cisplatin in a CRISPR screen for 27 genotoxic agents in RPE1 cells reported in Olivieri, et al.[21]. (**B**) NPEPPS mRNA is upregulated in response to cisplatin treatment in a dose-dependent manner in both KU1919-Par and KU1919-GemCis cells. Independent triplicate experiments are shown (mean ± SEM) (t-test compared to 0μM; *p < 0.05, **p < 0.05). (**C, E**) KU1919-GemCis or T24-GemCis cells with knockdown of NPEPPS treated with increasing doses of cisplatin or gemcitabine. A total of 3 technical replicates per dose (mean ± SEM). (**D**, **F**). KU1919 or T24 parental cells with overexpression of NPEPPS treated with increasing doses of cisplatin or gemcitabine. A total of 3 technical replicates per dose (mean ± SEM). Independent experiments are reported in **Figure S6**. p-values comparing IC50 values using sum-of-squares F test.

Volume regulated anion channels impact chemoresistance in bladder cancer cells

NPEPPS is one of 13, M1 aminopeptidases that cleaves amino acids from the N-terminus of polypeptides. NPEPPS is involved in cell growth, development, and antigen presentation[34–37]. A role for NEPPPS in chemotherapeutic response is newly described here. To begin characterizing the NPEPPS-mediated mechanisms of cisplatin resistance, we investigated NPEPPS protein interaction partners in the BioPlex interactome, a database that has collected affinity-purification mass spectrometry measurements of systematically over-expressed, tagged proteins[38]. Remarkably, among the small number of proteins that were observed to interact with NPEPPS, were all five subunits of the volume regulated anion channel (VRAC), leucine rich repeat containing 8 VRAC subunit A-E (LRRC8A-E) (**Figure 4A**). Equally interesting was that none of the other 12, M1 aminopeptidases were found in complex with any VRAC members in the BioPlex interactome. Additionally, none of the other 12, M1 aminopeptidases were found to be synthetic lethal in our CRISPR screens (**Table S5**). To examine if the NPEPPS-VRAC interaction is present in bladder cancer cell lines, we generated FLAG-tagged NPEPPS overexpressing KU1919 and T24 cells (**Figure 4B**). We immunoprecipitated against FLAG and performed immunoblotting against NPEPPS and LRRC8A, the obligate channel member[39]. We found that LRRC8A reliably co-immunoprecipitated with NPEPPS in both cell lines (**Figure 4C**). Additionally, using antibodies targeting the native protein, we pulled down NPEPPS and found LRRC8A, and complementary pulled down LRRC8A and found NPEPPS in the KU1919-GemCis cells (**Figure 4D**). To verify this relationship in a separate parental cell line, we pulled down NPEPPS and found LRRC8A in T24 parental cells (**Figure 4D**).

To gain insights into the functional domains important for the NPEPPS-VRAC interaction, we overexpressed a FLAG-tagged, mutant form of NPEPPS with an isoleucine residue (I) at the 440th position in the full-length NPEPPS protein, where a lysine residue (K) is located in the wildtype NPEPPS protein (**Figure 4E**). This position has been previously shown to be critical to the enzymatic domain of NPEPPS, and when mutated to isoleucine, affects NPEPPS structure to disrupt the active site[40]. We immunoprecipitated against FLAG and performed immunoblotting against NPEPPS and LRRC8A. We found that NPEPPS^{K440I} resulted in the disruption of the interaction with LRRC8A suggesting that NPEPPS-VRAC interaction is mediated through the active site of NPEPPS (**Figure 4E**).

VRACs directly respond to osmotic stress by trafficking osmolytes, such as chlorine, potassium, and taurine, across the plasma membrane to regulate cell volume[41]. Importantly, the VRAC channel is a hetero-hexamer of subunits that requires the presence of LRRC8A (SWELL1[39]) to function normally. This is particularly relevant since LRRC8A has been shown to mediate platinum drug resistance. Knockout experiments in kidney and colorectal cell lines showed that 50-70% of intracellular cisplatin is transported through these channels in isotonic conditions[4]. In addition to LRRC8A, LRRC8D, but not LRRC8B, LRRC8C, or LRRC8E, was shown to mediate cisplatin resistance. Similar findings were subsequently found in ovarian cancer and alveolar carcinoma cell lines[42–44]. Interestingly, we found that LRRC8D gene expression in the TCCSUP-Cis and TCCSUP-GemCis cells was completely lost as a consequence of a deep deletion at the LRRC8D locus (**Figure S7**). Thus, we focused on the LRRC8A and LRRC8D subunits for further analysis.

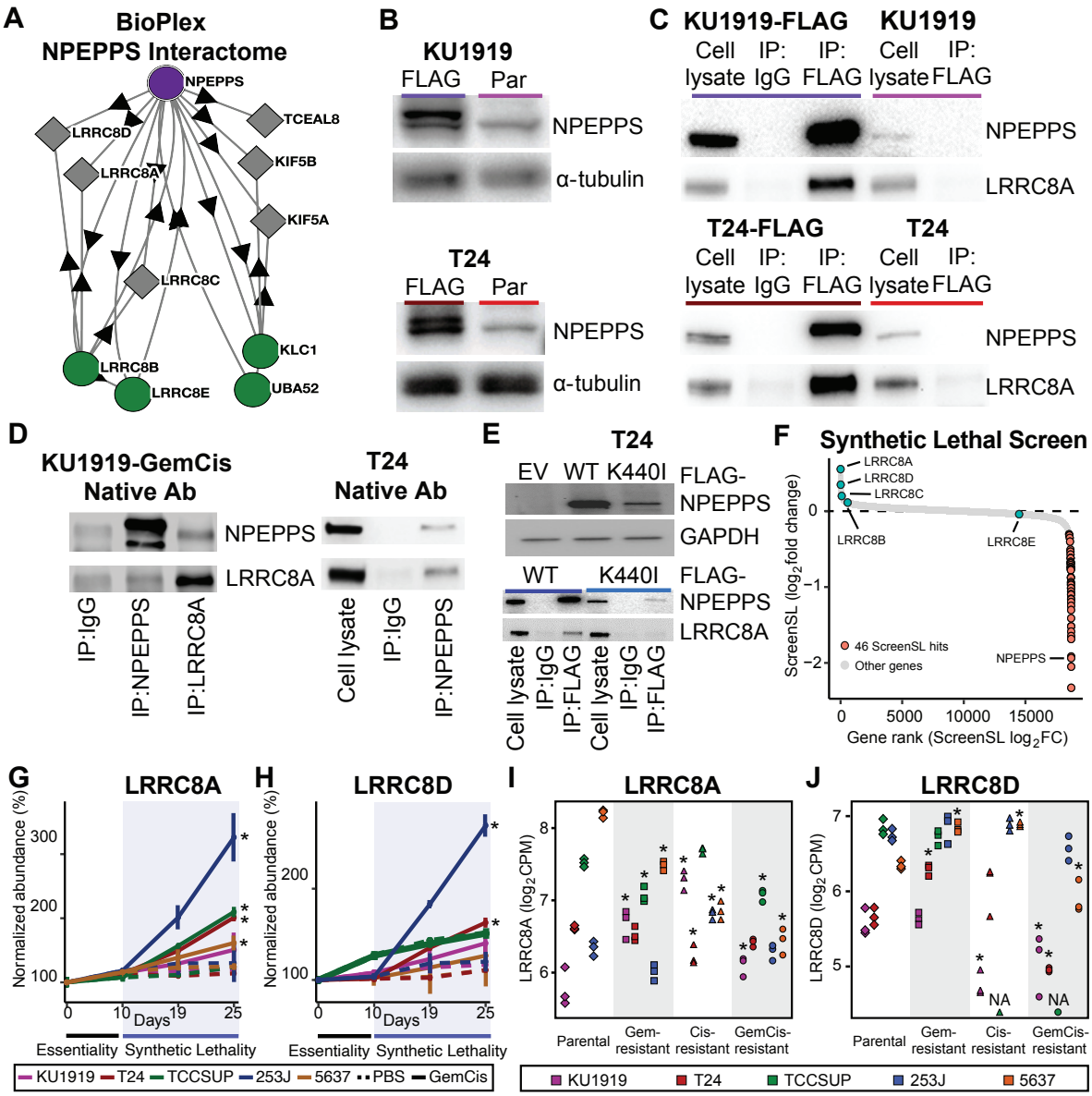

Figure 4. NPEPPS interacts with volume-regulated anion channel (VRAC) subunits LRRC8A and LRRC8D to mediate cisplatin response. (**A**) NPEPPS is found to interact with all VRAC subunits, LRRC8A-E, as reported in the BioPlex interactome[38]. (**B**) FLAG-tagged NPEPPS was overexpressed in KU1919 and T24 parental cell lines. (**C**) An anti-FLAG antibody was used against KU1919 and T24 parental cell lines as controls and overexpressing FLAG-tagged NPEPPS, KU1919, and T24 cells. The immunoprecipitant was immunoblotted for NPEPPS, LRRC8A, and LRRC8D, demonstrating that LRRC8A and LRRC8D are in complex with NPEPPS. (**D**) Pulldown of NPEPPS or LRRC8A was performed using the antibody to the native protein in the KU1919-GemCis or T24 parental cell lines. (**E**) FLAG-tagged wildtype NPEPPS (WT), empty vector control (EV), and K440I mutant NPEPPS were overexpressed in T24 cells. Immunoprecipitation against FLAG and immunoblotting against NPEPPS and LRRC8A was performed. (**F**) Genes were ranked based on $\log_2$ fold change from the synthetic lethal CRISPR screens across all cell lines. LRRC8A-E (teal) and the 46 common synthetic lethal genes (orange) are shown. (**G, H**) Knockout of LRRC8A and LRRC8D through the CRISPR screen resulted in increased cell growth upon gemcitabine plus cisplatin treatment in GemCis-resistant cell lines (mean ± SD; moderated t-test; *FDR < 0.05). (**I, J**) LRRC8A and LRRC8D gene expression measured by RNAseq (moderated t-test compared to parentals; *FDR < 0.05).

361 We revisited our CRISPR screens and RNAseq data to determine if loss of LRRC8A and/or
362 LRRC8D impacted cisplatin resistance. Strikingly, LRRC8A was the 1st and LRRC8D was the
363 11th ranked gene that when lost provided a growth advantage in gemcitabine plus cisplatin
364 treatment across all cell lines (**Figure 4F**). Individually, LRRC8A and LRRC8D loss provide a
365 growth advantage to cells treated with gemcitabine plus cisplatin (**Figure 4G,H**). LRRC8A
366 and/or LRRC8D mRNA expression was reduced for most of the Cis- or GemCis-resistant cell
367 lines, with the Gem-resistant lines showing variable differential expression (**Figure 4I,J**).
368 Notable, LRRC8D loss had no effect on treatment response in the TCCSUP-GemCis lines
369 (**Figure 4H**), which is consistent with the finding that LRRC8D is focally deleted in these lines
370 (**Figure S7**, **4J**). Additionally, NPEPPS loss in the TCCSUP-GemCis lines showed the weakest
371 synthetic lethal result compared to the other four GemCis-resistant lines (**Figure 2D**). Taken
372 together, these data support a functional dependency between NPEPPS and VRAC subunits
373 LRRC8A and LRRC8D in relation to cisplatin resistance.
374
375 Given that VRACs transport cisplatin and carboplatin[4] and finding NPEPPS in complex with
376 VRAC subunits (**Figure 4C,D**)[38,45,46], we hypothesized that NPEPPS may be a negative
377 regulator of VRAC activity, consequently reducing import of intracellular cisplatin. Thus, we
378 tested the impact of NPEPPS on osmolytes known to be transported through VRACs. NPEPPS
379 knockdown in KU1919-GemCis-shN39 cells resulted in significantly lower levels of intracellular
380 taurine, hypotaurine, creatine, phosphocreatine, and several other amino acids (**Figure 5A** and
381 **Table S11**), which are known to be exported via VRACs[4,41,47]. In addition, intracellular levels of
382 taurine were reduced even further when cells with knockdown of NPEPPS were also treated
383 with 10μM cisplatin (**Figure 5A**). Absolute quantification of taurine in T24-GemCis-shN39 cells
384 at 24 hours confirmed these findings (**Figure 5B**). These results suggest that cisplatin further
385 stimulates channel activity when NPEPPS is decreased, which allows for increased export of
386 taurine, and as we show next, increases cisplatin import.
387
388 To evaluate NPEPPS impact on cisplatin import, we directly measured intracellular cisplatin
389 using the metal ion detection capabilities of cytometry by time-of-flight, CyTOF[48]. We measured
390 intracellular cisplatin after 4 hours of treatment at 10μM across KU1919, 5637, and T24 cell
391 lines. Using KU1919 as the illustrative example, KU1919-GemCis cells (median Pt 195 = 102)
392 showed decreased uptake of cisplatin compared to KU1919-Par cells (median Pt 195 = 565).
393 Control knockdown had little effect (median Pt 195 = 121), but NPEPPS knockdown shifted the
394 intracellular levels of cisplatin to that of parent lines (median Pt 195 = 375), suggesting that
395 NPEPPS depletion allows for increased import of cisplatin (**Figure 5C** and **S8**). These findings
396 were repeated in the 5637 and T24 cell lines with highly similar results (**Figure 5C** and **S8).**
397
398 Furthermore, we measured protein levels of LRRC8A and LRRC8D after 48 hours of PBS or
399 10μM cisplatin treatment in NPEPPS knockdown or nontargeting control KU1919-GemCis,
400 5637-GemCis, and T24-GemCis cells. Supporting the CyTOF results (**Figure 5C**) and the result
401 that taurine is exported at a higher rate upon cisplatin stimulation in the GemCis-shN39 cells
402 (**Figure 5A, B**), NPEPPS knockdown increased DNA damage as measured by γH2AX foci
403 (**Figure 5D** and **S8E,F**). However, we did not find major changes in LRRC8A or LRRC8D
404 expression in response to NPEPPS knockdown or cisplatin treatment (**Figure 5D** and **S8E,F**).
405
406 To determine the functional relationship between expression of NPEPPS and VRACs on
407 intracellular cisplatin import, we performed a series of siRNA experiments targeting NPEPPS
408 and/or LRRC8A (**Figure S9A**), the obligate subunit for normal VRAC function as mentioned
409 above[39,41]. We found that knockdown of NPEPPS in KU1919 parental cells increased import of
410 cisplatin (KU1919 median Pt 195 = 1081; KU1919-siNPEPPS median Pt 195 = 1715) (**Figure**

411 **5E** and **S9B**); this finding is consistent with our results from the GemCis-resistant cells (**Figure**
412 **5C**). As expected, knockdown of LRRC8A resulted in decreased intracellular cisplatin (median
413 Pt 195 = 428), but knockdown of NPEPPS in combination with LRRC8A showed minimal
414 additional effect (median Pt 195 = 498) (**Figure 5E** and **S9B**). These findings were reproduced
415 in the 5637 and T24 cell lines (**Figure 5E** and **S9C,D)**. In addition, we performed the same
416 siRNA experiments on the GemCis-resistant derivative cells (**Figure S10A**). As expected,
417 depletion of LRRC8A did not result in additional resistance as these cells are already resistant,
418 while NPEPPS knockdown alone resulted in increased intracellular cisplatin (**Figure S10B-D**).
419 Loss of NPEPPS had no effect when LRRC8A was also depleted (**Figure S10B-D**).
420 Overexpression of NPEPPS in KU1919, 5637, and T24 parental cells resulted in decreased
421 intracellular cisplatin, suggesting that overexpression of NPEPPS is blocking cisplatin import
422 (**Figure S11**). Additionally, we verified that CRISPR knockout of NPEPPS, using a gRNA from
423 the CRISPR screen, resulted in increased import of cisplatin in cisplatin-resistant KU1919 cells.
424 Overexpressing NPEPPS in the knockout cells restored cisplatin import levels to the original
425 cisplatin-resistant cells (**Figure 5F**). Knockout and overexpression of NPEPPS was validated via
426 immunoblot and treatment response of these cells were consistent with shRNA targeting of
427 NPEPPS (**Figure S6D**). To evaluate how intracellular cisplatin levels were affected by the
428 $NPEPPS^{K440I}$ mutant presented in **Figure 4E**, we treated overexpressing control empty vector,
429 $NPEPPS^{K440I}$, and $NPEPPS^{WT}$ with cisplatin and found that $NPEPPS^{WT}$ was able to reduce
430 intracellular cisplatin, but $NPEPPS^{K440I}$ was not (**Figure S12**). These results are consistent with
431 the predicted effect given that the mutant disrupts the interaction with LRRC8A (**Figure 4E)**.
432 Finally, we tested if carboplatin showed the same patterns of NPEPPS-mediated cisplatin
433 import. Using KU1919 and T24 cells, we found the same patterns using carboplatin as we found
434 with cisplatin (**Figure S13**). All of these results support the role of NPEPPS in mediating
435 cisplatin import via the VRACs.
436
437 To validate the role of LRRC8D in cisplatin import, we measured intracellular cisplatin in the
438 TCCSUP cells and found that, as expected, the parental cells imported much more cisplatin
439 (median Pt 195 = 189) than the TCCSUP-GemCis cells (median Pt 195 = 22). In contrast to the
440 KU1919, 5637, and T24 cells (**Figure 5C**), NPEPPS knockdown had very little effect on the
441 GemCis-resistant cells (median Pt 195 = 28; **Figure 5G**) given that the TCCSUP-GemCis cells
442 have a focal deletion of LRRC8D (**Figure S7**). However, when we overexpressed LRRC8D,
443 cisplatin import was restored to the levels of the parental cell line (**Figure 5H**). Taken together,
444 these data support a mechanism by which NPEPPS controls cisplatin import and subsequence
445 cisplatin sensitivity through the VRACs.
446
447

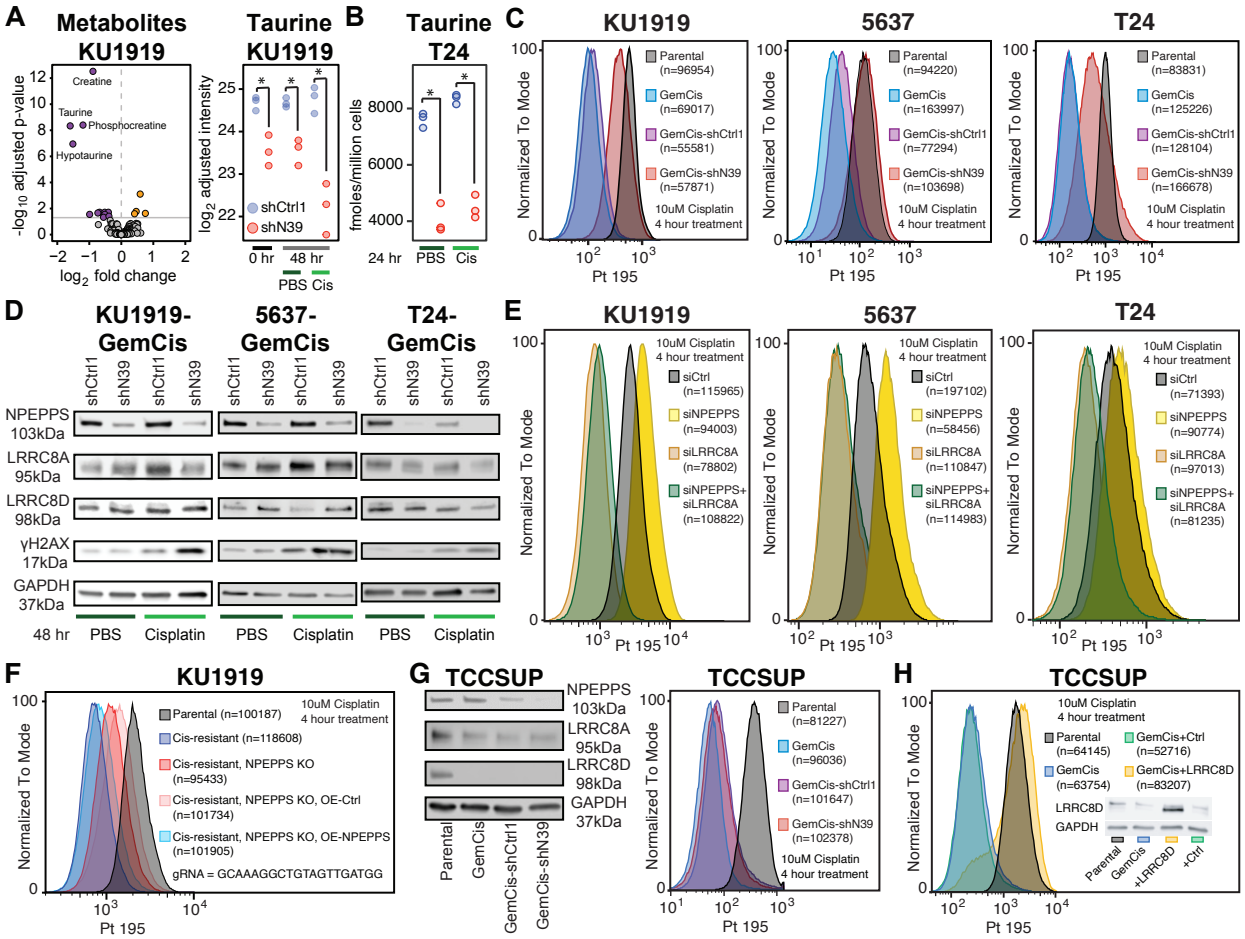

Figure 5. NPEPPS regulates VRAC activity and mediates cisplatin import. (**A**) Volcano plot of metabolites measured from KU1919-GemCis cells with or without NPEPPS knockdown (shN39). Time and treatment (cisplatin 10μM) were covariates in the linear model to calculate differential expression using a moderated t-test; the horizontal grey line is -$\log_{10}$(FDR = 0.05). (**B**) Taurine abundance was measured in KU1919-GemCis cells with non-targeting shRNA controls or shRNA targeting NPEPPS (shN39). Cells were also measured at 48 hours treated with 10μM cisplatin or PBS. (**C**) Intracellular cisplatin levels in KU1919, 5637, and T24 cells were measured after 4 hours of 10μM cisplatin treatment using CyTOF, with the number of cells analyzed as indicated. (**D**) Immunoblot of LRRC8A, LRRC8D, and γH2AX in cells treated with PBS or 10μM cisplatin for 48 hours. (**E**) Intracellular cisplatin concentrations were measured for KU1919, 5637, and T24 parental, untargeted knockdown (siCtrl), targeted knockdown of NPEPPS (siNPEPPS), LRRC8A (siLRRC8A), and the combination of NPEPPS and LRRC8A (siNPEPPS+siLRRC8A). (**F**) Intracellular cisplatin was measured in cisplatin-resistant KU1919 cells, the same resistant cells with CRISPR knockout of NPEPPS, and the NPEPPS knockout cells with overexpression of NPEPPS or empty vector control (OE-Ctrl). Cells were treated with 10μM cisplatin for 4 hours. (**G**) Immunoblot for NPEPPS, LRRC8A, and LRRC8D in parental TCCSUP cells, and as in (**C**), intracellular cisplatin was measured in parental, GemCis-resistant, control-knockdown, and NPEPPS knockdown TCCSUP cells. (**H**) TCCSUP-GemCis cells have a focal loss of LRRC8D (**Figure S10**). Intracellular cisplatin was measured in TCCSUP-GemCis cells with overexpression of LRRC8D. Immunoblot inset to verify overexpression of LRRC8D.

Genetic inhibition of NPEPPS enhances chemotherapy sensitivity *in vivo*

To test if NPEPPS depletion sensitizes tumor cells to gemcitabine plus cisplatin treatment *in vivo*, we established subcutaneous xenografts using the KU1919-GemCis cells with either NPEPPS shRNA knockdown or non-targeting shRNA control. When tumors reached roughly 200mm^3, mice were randomized into four groups: shCtrl1 with PBS (n=11), shCtrl1 with gemcitabine plus cisplatin (n=11), shN39 with PBS (n=11), and shN39 with gemcitabine plus cisplatin (n=12). Treatment was delivered through intraperitoneal injection, with PBS or gemcitabine plus cisplatin administered three times weekly for four weeks. Tumor volumes were monitored until they reached the predetermined endpoint of 2cm^3. NPEPPS knockdown alone and gemcitabine plus cisplatin treatment alone had significant impact on tumor growth compared to vehicle-treated, shRNA controls. The combination of NPEPPS knockdown and gemcitabine plus cisplatin treatment led to a stronger and significant impact on tumor growth (**Figure 6A**). We further analyzed tumor growth using linear mixed-effects models aimed at capturing trends in tumor volume change in relation to pre-treatment baseline tumor volume across the four groups (**Figure S14A,B**). According to this model, tumor growth inhibition by NPEPPS knockdown (p=0.00178), GemCis treatment (p=5.49e-7), or the combination of NPEPPS knockdown and gemcitabine plus cisplatin treatment (p=1.47e-8) were all consistent effects over the treatment period compared to PBS treated control tumors (**Figure 6A,B**). We validated NPEPPS knockdown in the pre-xenograft inoculate cells and after tumors were removed from mice upon reaching the 2cm^3 endpoint (**Figure S14C**). Survival analysis using tumor volume as the endpoint showed that mice treated with gemcitabine plus cisplatin had a 14-day survival advantage. Similarly, knockdown of NPEPPS resulted in a 14-day survival advantage. Mice treated with gemcitabine plus cisplatin and with NPEPPS knockdown tumors had a 25-day survival advantage, a statistically significant improvement (Logrank test, $p<0.0001$) (**Figure 6B, S14D**).

The increase in NPEPPS mRNA that has been observed in response to chronic (**Figure 2B,C**) and acute cisplatin treatment *in vitro* (**Figure 3B**) suggests that high levels of NPEPPS expression are part of an acquired or adaptive rather than intrinsic mechanism of drug resistance in tumors that have been exposed to cisplatin. Hence, pre-treatment tumor NPEPPS levels may not necessarily be a biomarker of chemotherapy response in bladder cancer. This prediction is consistent with NPEPPS gene expression patterns using TCGA data from muscle-invasive bladder cancer[24]. We stratified patients with and without a record of platinum-based treatment[18] into low and high NPEPPS expressing groups (median stratification) and found no difference in overall survival (**Figure S15**). However, given the relationship of NPEPPS to VRACs that we describe here and findings that levels of LRRC8A and LRRC8D are predictive of cisplatin response in ovarian cancer[4], we reasoned that such relationships would also be true in BCa. Using the same TCGA data, we compared patients with and without a record of platinum-based treatment[18] with respect to amplification, copy number, and expression of LRRC8A or LRRC8D. Notably, patients with LRRC8A or LRRC8D copy number gain or overexpression that received cisplatin-based treatment showed significantly improved overall survival in contrast to those with no record of this treatment modality (**Figure 6C,D**). Together, these findings support VRAC subunits LRRC8A and LRRC8D as pre-treatment biomarkers of response to cisplatin-based chemotherapy[2].

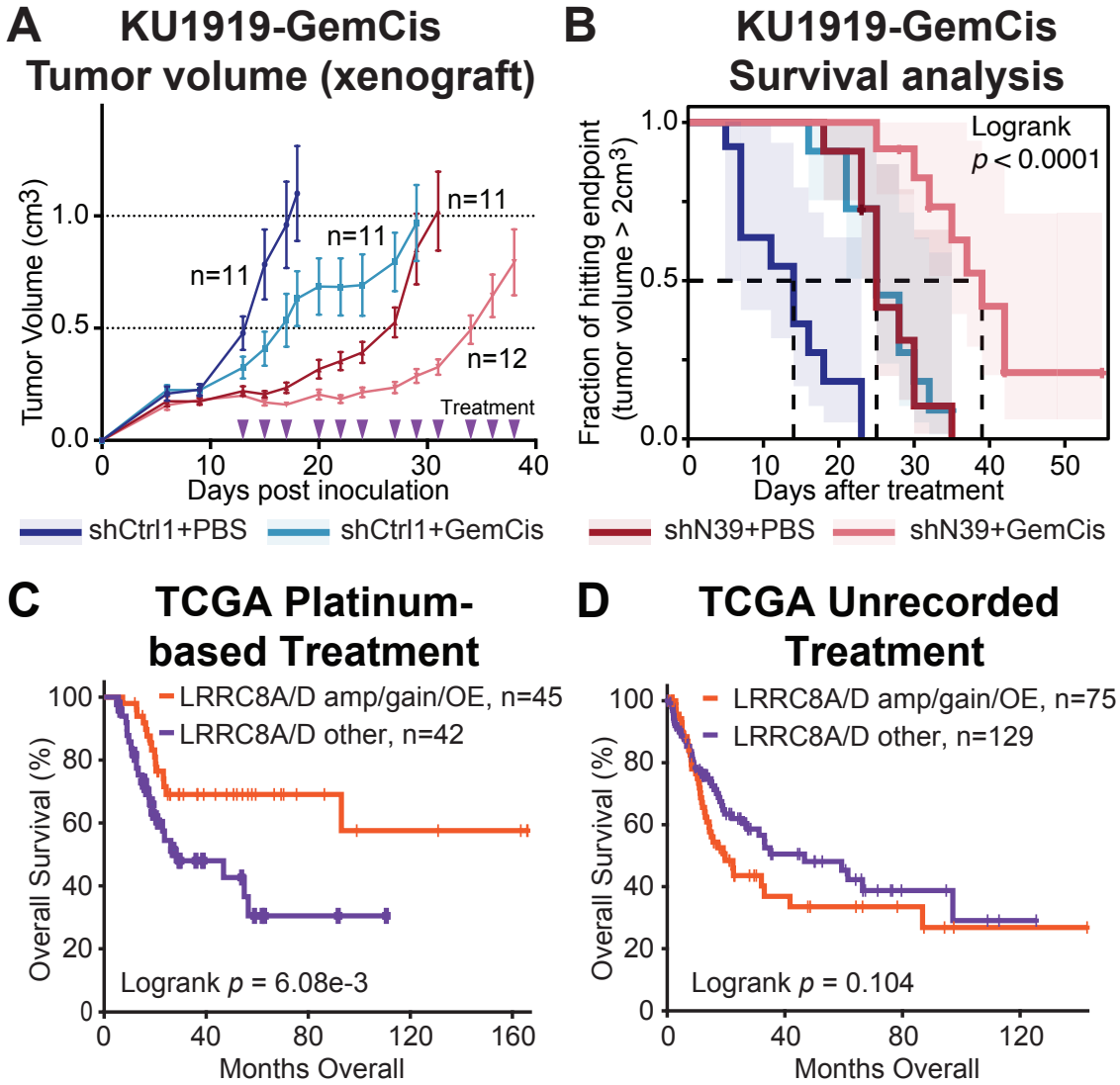

Figure 6. NPEPPS effect *in vivo* and LRRC8A/D is a biomarker in patients. (**A**) Tumor volume (mean ± SEM) of KU1919-GemCis xenografts measured over time and across 4 treatment groups considering non-targeting shRNA controls (shCtrl1), shRNA targeting NPEPPS (shN39), PBS vehicle control (PBS), or gemcitabine plus cisplatin treatment (GemCis). (**B**) Survival analysis of xenograft models with a defined endpoint of a tumor volume > $2cm^3$. Logrank test was applied to test significance. (**C**) Survival analysis of muscle-invasive bladder cancer in the TCGA stratified based on copy number amplification, gain or overexpression of LRRC8A or LRRC8D. Patients all had a record of cisplatin-based chemotherapy treatment. (**D**) Survival analysis for patients stratified by LRRC8A or LRRC8D as in (**C**), but that did not have any record of cisplatin-based treatments.

DISCUSSION

NPEPPS has been suggested to play a role in a range of cellular processes including promoting autophagy, regulating cell cycle progression, and antigen processing[34–37]. The majority of what is known about NPEPPS has been from studies in the brain, where it targets the degradation of polyglutamine sequences and misfolded protein aggregates associated with a number of neurodegenerative diseases, including Alzheimer's disease, Huntington's disease, and Parkinson's disease[37,49–52]. As reported in gnomAD, NPEPPS is a highly conserved gene and is constrained based on several metrics of intolerance to genetic variation in the population[53]. NPEPPS is also ubiquitously expressed across human tissues[54]. However, despite these features, genetic modification in mice is tolerable, though mice are slower growing, more sickly, and sterile[36,55], and as we have shown from our CRISPR screen results and follow-up experiments, knockout is not essential for growth in bladder cancer cells (**Figure 2D, 5F, S6**). Overall, our results demonstrate that genetic downregulation of NPEPPS re-sensitizes treatment-resistant cells back to cisplatin and the mechanism by which NPEPPS controls intracellular import is through VRACs.

Our results support the role of NPEPPS as an interaction partner that controls cisplatin-based response in BCa via VRACs, thus we have scoped our conclusions accordingly. However, results outside of this study suggest a molecular mechanism with broader impact. The evidence that supports the interaction between NPEPPS and VRACs was derived from several different cell types and the evidence that implicates VRACs in platinum-based chemotherapy sensitivity is from ovarian cancer[4,42–44]. If the NPEPPS-VRAC mechanism of platinum-based chemotherapy resistance is a general mechanism, then there are clear implications for any cancer type that uses platinum-based treatments. Hence, we propose a model (**Figure 7**) where a cancer cell imports cisplatin, which in turn causes DNA damage and eventually cell death. An inherent mechanism of resistance can simply be the number of VRACs in a tumor cell, where downregulation of VRAC subunits can lead to treatment resistance, such as was previously found in ovarian cancer, or the opposite effect seen with LRRC8A or LRRC8D upregulation in BCa (**Figure 6C,D**). In our model, NPEPPS interacts with LRRC8A and/or LRRC8D to inhibit channel activity, thus providing resistance to cisplatin and overall chemoresistance. If proven to be true, our insight into this mechanism opens up opportunities for novel therapeutic strategies to reverse or prevent the development of cisplatin resistance.

All of our data suggest that NPEPPS is a viable therapeutic target. Interestingly, while previous attempts at targeting drug efflux in the clinical setting have had disappointing results[56–58], the paradigm shift that our results suggest is increasing drug import could be a more effective therapeutic target. Direct targeting of the VRACs would result in blocking of platinum drug import and thus chemoresistance, but inhibition of NPEPPS would results in increased platinum drug import and potentially increased treatment response. Broadly, aminopeptidases have been therapeutically targeted as potential cancer treatments[59]. More specifically, NPEPPS is a zinc-containing M1 aminopeptidase. Tosedostat was developed as a target of M1 aminopeptidases and the intracellular metabolized product CHR-79888 is the most potent inhibitor of NPEPPS reported[60,61]. There have been a total of 11 clinical trials with tosedostat as reported in *clinicaltrials.gov*[60,62–65]. The focus of its application has been in leukemias and myelomas, with several applications in solid tumors. The few clinical trials completed have reported tosedostat as being well tolerated by patients, but with modest effect as a single agent cancer treatment. A few examples of tosedostat in combination with cytarabine, azacitidine, capecitabine or paclitaxel have been tried, but there are no reports of tosedostat being tried in combination with platinum-based chemotherapy. Future work will include the evaluation of tosedostat in combination with cisplatin-based chemotherapy.

579
580 Another exciting potential application of NPEPPS inhibition is to provide alternative treatment
581 options for BCa patients. Many patients are ineligible for cisplatin-based chemotherapies,
582 leaving them with less effective options, such as carboplatin. VRACs also transport carboplatin
583 at similar amounts as cisplatin[4], thus combining an NPEPPS inhibitor, such as tosedostat, with
584 carboplatin could provide a more effective and less toxic drug combination option for cisplatin-
585 ineligible patients. A further area of novel development would be the impact of NPEPPS
586 inhibition on ICT with its known effect on MHC class I antigen presentation on dendritic cells[36].
587 ERAP1 and ERAP2, other M1 aminopeptidases in the same family as NPEPPS, have been
588 linked to boosting T cell and NK cell-mediated immune response in cancer[66]; however the
589 impact of NPEPPS on antigen presentation in tumor cells is yet to be investigated. Interestingly,
590 low ERAP2 was associated with improved response to anti-PD-L1 in luminal bladder cancer[67].
591 The impact of NPEPPS inhibition on immunotherapies or in combination with platinum drugs will
592 be the subject of future studies.
593
594 This work is not without its limitations. We have shown in multiple settings that inhibiting
595 NPEPPS genetically results in re-sensitizing resistant BCa cells to cisplatin. However, where
596 and when NPEPPS interacts with VRACs in the cell is yet to be determined. In addition,
597 NPEPPS could have effects on treatment response outside of the VRACs. For example,
598 NPEPPS is upregulated in the Gem-resistant cell lines (**Figure 2**), and while we show that
599 genetic NPEPPS loss is specific to cisplatin response (**Figure 3, S6**), NPEPPS upregulation
600 could be part of broader cellular stress responses. Further studies will be needed to test other
601 NPEPPS-mediated mechanisms of stress response. We note that all of our data support a cell
602 autonomous effect of NPEPPS. As we indicated above, NPEPPS has been linked to
603 mechanisms of immune response and non-cell autonomous effects of NEPPS were not tested
604 here. Finally, in depth studies of pharmacological inhibition of NPEPPS *in vitro* and *in vivo* will
605 be needed to translate the mechanistic findings presented here into the pre-clinical and clinical
606 settings. Despite these study limitations, the implications of NPEPPS as a therapeutic target for
607 better treatment response has the potential to be translated into novel treatment regimens for
608 improved patient outcomes.
609
610 In conclusion, our finding that NPEPPS mediates cisplatin-based chemoresistance is both novel
611 and actionable. Cisplatin-based chemotherapeutic regimens are mainstays of treatment across
612 many cancer types and these novel findings lay the groundwork for improved treatment of
613 patients harboring these tumors[2]. Our findings also have implications into other platinum agents,
614 such as carboplatin which would further improve efficacy of this agent in additional cancer
615 types. Finally, for the benefit of the research community, we make the -omic and CRISPR
616 screen data publicly available through an R Shiny app to provide a rich source for novel analysis
617 in the mechanisms of chemotherapy resistance
618 (https://bioinformatics.cuanschutz.edu/BLCA_GC_Omics/).
619

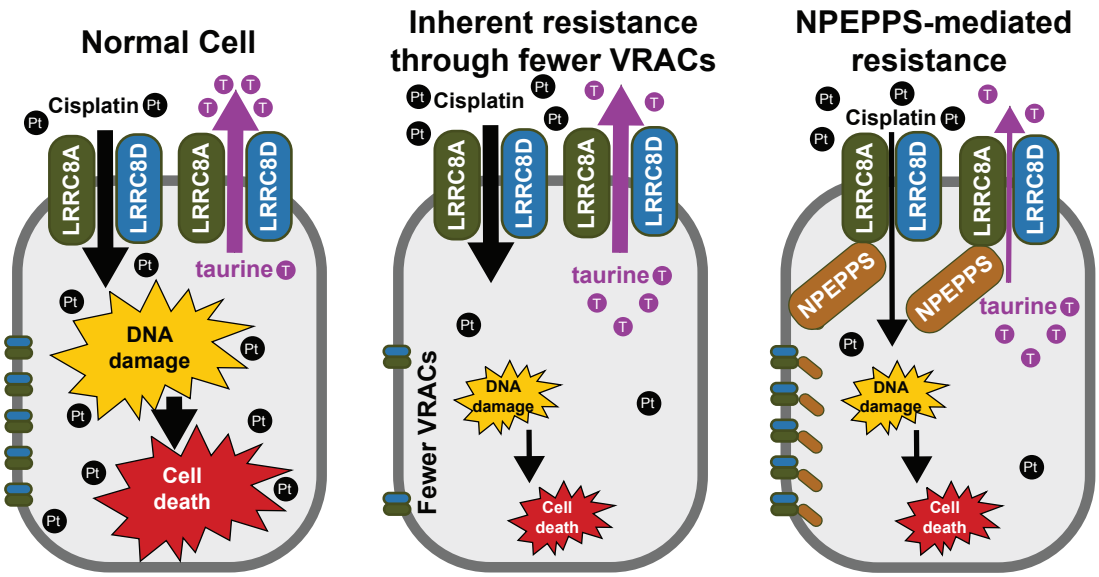

Figure 7. Proposed model of NPEPPS-mediated cisplatin resistance. Normal functioning cells will import cisplatin through the volume-regulated anion channels (VRAC), with LRRC8A and LRRC8D being the primary subunits. A mechanism of cisplatin resistance is to inherently down-regulate VRACs. We propose that NPEPPS interacts with LRRC8A or LRRC8D directly to decrease VRAC activity, which prevents the export of taurine and import of cisplatin, hence driving cisplatin resistance.

627 **Materials and Methods**
628
629 **Cell Culture**

630 All human BCa cell lines as reported in the Key Resource Table were obtained from the
631 Resistant Cancer Cell Line (RCCL) Collection and were grown in Iscove's Modified Dulbecco's
632 Medium (IMDM) with 10% Fetal Bovine Serum (FBS). Cells were passaged every two to three
633 days. Resistance to gemcitabine and cisplatin were confirmed at the reported resistance doses
634 from the RCCL (**Table S1** and **Figure S1**). Lentivirus production utilized 293FT cells
635 (ThermoFisher), which were maintained in DMEM (high glucose) supplemented with 0.1mM
636 non-essential amino acids (NEAA), 6mM L-glutamine, 1mM sodium pyruvate, and 500μg/mL
637 geneticin (G418) with 10% FBS added. Cells were routinely monitored for mycoplasma and
638 confirmed negative at multiple times during this study using MycoAlert (Lonza). All cells were
639 grown at 37°C with 5% CO_2 in a humidified incubator.

640 All molecular characterization efforts (RNA sequencing, whole exome sequencing, and mass
641 spectrometric proteomics) were performed on cells from independent passages and in drug-
642 free, complete media to identify stable molecular changes rather than treatment-induced
643 transient responses. Cells were routinely passaged through drug-containing media at the
644 resistant doses (**Table S1**) to confirm resistance was maintained and early passage cells were
645 utilized whenever possible.

646

647 **RNA sequencing**

648 ***Sample preparation***

649 All cell lines were grown for several passages in the absence of antibiotics, gemcitabine or
650 cisplatin. Cell pellets were snap frozen from sub-confluent dishes from 3 separate passages
651 (replicates) for each of the 20 cell lines sequenced (5 cell lines, each with 4 derivatives:
652 parental, G-resistant, C-resistant, GC-resistant). RNA was extracted using the RNAeasy Plus
653 Kit (Qiagen). Cells were lysed and passed through QIAShredder column (Qiagen) according to
654 the manufacturer's protocol. gDNA elimination columns (Qiagen) were used to remove any
655 residual gDNA from the purified RNA. RNA integrity was assessed on the High Sensitivity
656 ScreenTape Assay on the Tape Station2200 (Agilent) and only samples with an RIN score of 8
657 or higher were used for sequencing. RNA library preparation was performed using the Universal
658 Plus mRNA –Seq +UDI kit (Nugen) according to the manufacturer's specification. Each library
659 was sequenced to a minimum of 40 million clusters or 80 million 150bp paired-end reads on a
660 NovaSeq 6000 instrument (Illumina) at the University of Colorado Cancer Center Genomics
661 Shared Resource.

662 ***Data processing***

663 Illumina adapters and the first 12 base pairs of each read were trimmed using BBDuk and reads
664 <50bp post trimming were discarded. Reads were aligned and quantified using STAR[68] against
665 the Ensembl human transcriptome (GRCh38.p12 genome (release 96)). Ensembl genes were
666 mapped to HGNC gene symbols using HGNC and Ensembl BioMart. Gene counts were
667 generated using the sum of counts for transcripts of the same gene. Lowly expressed genes
668 were removed if mean raw count <1 or mean CPM (counts per million) <1 for the entire dataset.
669 Reads were normalized to CPM using the edgeR R package[69]. Differential expression was
670 calculated using the voom function in the limma R package[70]. In addition to two-group
671 comparisons, single drug comparisons for all cell lines were generated with cell line as a
672 covariate (**Table S9**).

673 ***Alignment and transcript quantification***

674 STAR --runThreadN 12 --runMode genomeGenerate --sjdbGTFfile
675 Homo_sapiens.GRCh38.96.gtf --genomeFastaFiles
676 Homo_sapiens.GRCh38.dna_sm.primary_assembly.fa
677
678 STAR --readFilesIn Read1.fastq.gz Read2.fastq.gz --readFilesCommand zcat --runThreadN 6 --
679 alignEndsProtrude 13 ConcordantPair --outFilterScoreMinOverLread 0.66 --
680 outFilterMatchNminOverLread 0.66 --outSAMtype BAM SortedByCoordinate --quantMode
681 GeneCounts
682

683 **Pathway analysis**

684 Gene set enrichment analysis was performed using the full list of genes ranked by fold change
685 for the indicated comparison and the fgsea R package[71] using gene sets from the Molecular
686 Signatures Database (v7.0)[72]. General plots were generated with the ggplot2 and ggpubr R
687 packages[73]. Heatmaps were generated with the ComplexHeatmap R package following z-score
688 transformation[74].

689

690 **Proteomics**

691 ***Sample preparation***

692 All cell lines were grown for several passages in the absence of antibiotics, gemcitabine or
693 cisplatin, then seeded at 100,000 – 200,000 cells per well and grown for 48 hours in IMDM +
694 10% FBS. Approximately 48 hours after seeding cells the supernatant was aspirated and cells
695 were washed 3 times with cold phosphate buffered saline (PBS). Cells were lysed in 100μl of
696 8M Urea, 50mM Tris-HCl, pH 8.0. Lysates were transferred to pre-chilled 1.5mL microcentrifuge
697 tubes and centrifuged at 15000 RCF for 10 minutes to pellet. The supernatant was then
698 transferred to a clean, pre-chilled tube and frozen. Lysate replicates were collected in triplicate
699 from different passages. Cell pellets were lysed in 8M Urea supplemented with 0.1% Rapigest
700 MS compatible detergent. DNA was sheared using probe sonication, and protein concentration
701 was estimated by BCA (Pierce, Thermo Scientific). A total of 30μg protein per sample was
702 aliquoted, and samples were diluted to <2M Urea concentration using 200mM ammonium
703 bicarbonate while also undergoing reduction with DTT (10mM) and then alkylation with IAA
704 (100mM). The pH of diluted protein lysates was verified as between 7-8, and samples were
705 digested with sequencing grade Trypsin/Lys-C enzyme (Promega) in the presence of 10%
706 Acetonitrile for 16 hours at 37°C. Samples were acidified adding formic acid to 1%, and speed
707 vac dehydration was used to evaporate acetonitrile. Peptides were desalted on C18 tips (Nest
708 group) and dried to completion. Prior to MS, peptides were resuspended in 0.1% Formic Acid
709 solution at 0.5μg/μL concentration with 1:40 synthetic iRT reference peptides (Biognosys).

710 ***Data acquisition***

711 Peptides were analyzed by liquid chromatography coupled with mass spectrometry in data
712 independent acquisition (DIA) mode essentially as described previously[75]. Briefly, 4μL of
713 digested sample were injected directly unto a 200 cm micro pillar array column (uPAC,
714 Pharmafluidics) and separated over 120 minutes reversed phase gradient at 1200 nL/min and
715 60°C. The gradient of aqueous 0.1% formic acid (A) and 0.1% formic acid in acetonitrile (B) was
716 implemented as follows: 2% B from 0 to 5 min, ramp to 4% B at 5.2 minutes, linear ramp to 28%
717 B at 95 minutes, and ramp to 46% B at 120 minutes. After each analytical run, the column was
718 flushed at 1200 nL/min and 60°C by injection of 50% Methanol at 95% B for 25 minutes followed

719 by a 10 minutes ramp down to 2% B and a 5 minute equilibration to 2% B. The eluting peptides
720 were electro sprayed through a 30 um bore stainless steel emitter (EvoSep) and analyzed on an
721 Orbitrap Lumos using data independent acquisition (DIA) spanning the 400-1000 m/z range.
722 Each DIA scan isolated a 4 m/z window with no overlap between windows, accumulated the ion
723 current for a maximum of 54 seconds to a maximum AGC of 5E5, activated the selected ions by
724 HCD set at 30% normalized collision energy, and analyzed the fragments in the 200-2000m/z
725 range using 30,000 resolution (m/z = 200). After analysis of the full m/z range (150 DIA scans) a
726 precursor scan was acquired over the 400-1000 m/z range at 60,000 resolution.

727 ***Peptide library generation***

728 To construct a comprehensive peptide ion library for the analysis of human BCa we combined
729 several datasets, both internally generated and external publicly available data resources were
730 utilized. First, we utilized a previously published[76] human bladder tumor proteomics experiment
731 by downloading raw files from the online data repository (ProteomeXchange, PXD010260) and
732 searching them through our internal pipeline for data dependent acquisition MS analysis[77]
733 against the UniProt human reviewed canonical sequence database, downloaded July 2019,
734 using internal peptides to perform retention time alignment[78]. To this library, we appended a
735 sample specific library generated from DIA-Umpire extraction of pseudo-spectra from one full
736 set of replicates from the experimental bladder tumor cell lines. A final, combined consensus
737 spectrast library containing all peptide identifications made between the internal and external
738 dataset was compiled and decoy sequences were appended.

739 ***Data analysis***

740 Peptide identification was performed as previously described in[77,78]. Briefly, we extracted
741 chromatograms and assigned peak groups using openSWATH[79] against the custom BCa
742 peptide assay library described above. False discovery rate for peptide identification was
743 assigned using PyProphet[80] and the TRIC[81] algorithm was used to perform feature-alignment
744 across multiple runs of different samples to maximize data completeness and reduce peak
745 identification errors. Target peptides with a false discovery rate (FDR) of identification <1% in at
746 least one dataset file, and up to 5% across all dataset files were included in the final results. We
747 used SWATH2stats to convert our data into the correct format for use with downstream software
748 MSstats[82]. Each individual data file was intensity normalized by dividing the raw fragment
749 intensities by the total MS2 signal. MSstats[82] was used to convert fragment-level data into
750 protein-level intensity estimates via the 'quantData' function, utilizing default parameters with the
751 exception of data normalization, which was set to 'FALSE'. For plotting purposes, protein
752 intensities were VSN normalized, log-transformed, and replicate batch effects were removed
753 using the removeBatchEffect function in the limma R package. The limma package was also
754 used to calculate differential protein expression[70]. Multiple hypothesis correction was performed
755 using the Benjamin Hochberg method.

756

757 **Whole exome sequencing**

758 ***Sample preparation***

759 All cell lines were grown for several passages in the absence of antibiotics, gemcitabine, or
760 cisplatin. Cell pellets were snap frozen from sub-confluent dishes for each of the 20 cell lines
761 sequenced (5 cell lines, each with 4 derivatives: parental, Gem-resistant, Cis-resistant, GemCis-
762 resistant). gDNA isolation was performed using the Puregene cell and tissue kit (Qiagen) with
763 the addition of RNase A Solution (Qiagen) according to manufacturer's instructions. gDNA was
764 quantified using a Qubit 4.0, then sheared using a Covaris S220 Sonicator to 200bp. Libraries
765 were constructed using the Sure Select All Exon v6 library kit (Agilent) following the XT library

preparation workflow. Completed libraries were run on the 4200 Tape Station (Agilent) using D1000 screen tape. Libraries were quantitated using the Qubit, diluted to 4nM prior to verification of cluster efficiency using qPCR, then sequenced on the NovaSeq 6000 instrument (Illumina) (150bp, paired-end) at the University of Colorado Cancer Center Genomics Shared Resource. Mean insert size across all cell lines was 177.8 bp and mean coverage was 193.7X with > 96.8% at >30X. Individual call line quality control metrics are reported in **Table S13**.

Data processing

The analysis pipeline was developed using Nextflow. For the raw fastq files, Fastqc was used to assess overall quality. For computational efficiency, raw sequence reads were partitioned using BBMap (partition.sh) into 40 partitions. They then were aligned to the GRCh38 reference genome (including decoy sequences from the GATK resource bundle) using the BWA-MEM short read aligner[83], and merged back into single BAM files using Samtools. The resulting BAM files were de-duplicated using Samblaster[84], and sorted using Samtools. These duplicate-marked bams were further passed through the GATK Base Quality Score Recalibration in order to detect systematic errors made by the sequencing machine when it estimates the accuracy of base calls. The dbSNP (version 146)[85], the 1000 Genome Project Phase 1[86], and the Mills and 1000G gold standard sets[87] were used as databases of known polymorphic sites to exclude regions around known polymorphisms from analysis. After alignment, Samtools[88], Qualimap[89], and Picard tools[90] were run to acquire various metrics to ensure there were no major anomalies in the aligned data.

Alignment

```
bwa mem -K 100000000 -R "read_group" -t 64 -M ref_fasta read_1 read_2
```

Marking duplicates

```
samtools sort -n -O SAM sample_bam | samblaster -M --ignoreUnmated
```

Base Quality Score Recalibration

```
gatk BaseRecalibrator -I sample_bam -O sample.recal.table -R ref_fasta --known-sites
known_sites
```

Whole exome sequencing variant calling

We used Mutect2 from the GATK toolkit for SNVs and short indels[91]. Mutect2 is designed to call somatic variants and makes no assumptions about the ploidy of samples. It was run in *tumor-only* mode to maximize the sensitivity albeit at the risk of high false positives. We used tumor-only mode to call variants for each cell line separately. Mutect2 workflow is a two steps process. In the first step, it operates in high sensitivity mode to generate intermediate callsets that are further subjected to filtering to generate the final variant calls. Annotation of variants was performed using Annovar[92] with the following databases: refGene, cytoBand, exac03, avsnp150, clinvar_20190305, gnomad211_exome, dbnsfp35c, cosmic90. Intergenic variants were removed along with variants that were identified at greater than 0.001% of the population according to ExAC or gnomAD, or had a depth < 20.

Mutect2 raw callset:

```
gatk Mutect2 -R ref_fasta -I bam_tumor -tumor Id_tumor --germline-resource germline_resource
-O raw_vcf
```

Mutect2 filtering:

```
gatk FilterMutectCalls -V raw_vcf --stats raw_vcf_stats -R ref_fasta -O filtered_mutect2_vcf
```

809 ***Copy number calling using GATK***

810 Base quality score recalibrated bams were used as the input. The covered regions for the
811 exome kit were converted into bins (defining the resolution of the analysis) for coverage
812 collection. Read-counts, that form the basis of copy number variant detection, were collected for
813 each bin. The read-counts then go through denoising, modelling segments, and calling the final
814 copy ratios.

815 ***Preprocess intervals***

816 gatk PreprocessIntervals --intervals intervals_bed_file --padding 0 --bin-length 0 -R ref_fasta --
817 interval-merging-rule OVERLAPPING_ONLY -O preprocessed_intervals_list

818 ***Collect read counts***

819 gatk CollectReadCounts -I sample_bam -L preprocessed_intervals} --interval-merging-rule
820 OVERLAPPING_ONLY -O sample.counts.hdf5

821 ***Denoise read counts***

822 gatk DenoiseReadCounts -I sample.counts.hdf5 --standardized-copy-ratios
823 sample_std_copy_ratio --denoised-copy-ratios sample_denoised_copy_ratio

824 ***Model Segments***

825 gatk ModelSegments --denoised-copy-ratios denoised_copy_ratio --output-prefix id_sample -O
826 output_dir

827 ***Call copy ratio segments***

828 gatk CallCopyRatioSegments -I sample.modelled_segments -O sampled.called.segments

829 ***Cell line authentication***

830 Variant calls from the Mutect2 pipeline were filtered for each cell line to identify high confidence
831 variants according to the filtering criteria above. These high confidence variants were then
832 compared to the variants reported for all cell lines in the DepMap (https://depmap.org/portal/) for
833 the Cancer Cell Line Encyclopedia (CCLE_mutations_hg38.csv, sample_info.csv) and COSMIC
834 (CosmicCLP_MutantExport.tsv) as measured by the jaccard distance, the intersection of
835 variants divided by the union of variants. Cells listed in CCLE or COSMIC were the rank ordered
836 for each BCa cell line in this study according to the jaccard distance. Results are reported in
837 **Table S14**.

838

839 **Metabolomics**

840 ***Sample preparation***

841 Cell lines were cultured for several passages in IMDM + 10% FBS (IMDM10). Prior to
842 experiment, cells were cultured in IMDM10 to ~80% confluence and then dissociated. For
843 dissociation, cells were washed once with room temperature PBS and then incubated with PBS
844 + 0.05% Trypsin-EDTA for 10-15 minutes. Cells were neutralized with IMDM10 and then fully
845 dissociated by gentle pipetting. After dissociation, cells were counted by Trypan blue staining
846 and then replated at 1e6 cells. 24 hours after plating, cells were treated with either IMDM10 or
847 IMDM10 + 10μM cisplatin. Day 0 cell cultures were immediately processed for metabolomics
848 analysis. To prepare cell pellets for metabolomics analysis, day 0 cells were dissociated and
849 then centrifuged at 300RCF for 10 minutes at 4°C. Cells were suspended in PBS, centrifuged a
850 second time, and then resuspended in PBS and counted. Day 0 cells were centrifuged a third
851 time, the supernatants were aspirated, and the dry cell pellets were snap frozen in liquid

852 nitrogen and stored at -80°C until metabolite extraction. 48 or 72 hours after plating, cells were
853 processed for metabolomics analysis as described for the day 0 cell cultures.

854 ***Data generation and analysis***

855 Metabolites from frozen cell pellets were extracted at 2e6 cells/mL in ice cold 5:3:2
856 MeOH:acetonitrile:water. For absolute quantification of taurine, samples were supplemented
857 with 1 uM $^{13}C_2$, ^{15}N taurine (Cambridge Isotope Laboratories #CNLM-10253). Samples were
858 vigorously vortexed (30 min, 4°C) and clarified by centrifugation (10 min, 18,000 g 10, 4°C). 10
859 μL metabolite extract was analyzed using a Thermo Vanquish UHPLC coupled to a Thermo Q
860 Exactive mass spectrometer. Global metabolomics analyses were performed using a 5 min C18
861 gradient in positive and negative ion modes (separate runs) with electrospray ionization as
862 described in[93,94]. For all analyses, the MS scanned in MS^1 mode across the m/z range of 65 to
863 950. Peaks were annotated in conjunction with the KEGG database, integrated, and quality
864 control was performed using Maven as described in[95]. Data was variance stabilization
865 normalized[96], log2-transformed, and differential abundance calculations were done using
866 limma[70] with time and/or treatment as covariates in the linear model. Absolute quantification of
867 taurine was performed according to the following equation:
868
869 $[\text{taurine}]_{\text{cells}}$ = (endogenous peak area)/($^{13}C_2$, ^{15}N taurine peak area)(1 uM)(1 mL/2e6 cells)
870

871 **Cell Line Drug Treatments**

872 Gemcitabine (Sigma) and cisplatin (Sigma) stocks were resuspended in 0.9% saline solution. All
873 stocks solutions were stored protected from light and kept frozen until use. For cell culture dose
874 response, cells were seeded in 96-well tissue culture plates with 500-2000 cells per well
875 depending on growth rate and duration of experiment. Cells were seeded and allowed to attach
876 overnight followed by replacing the media with fresh, pre-warmed media just prior to treatment.
877 Drug dilutions were performed serially and using complete media (IMDM + 10% FBS) and the
878 associated drug treatments. Growth inhibition was measured using confluence estimates over
879 time on the IncuCyte ZOOM (Essen Bioscience) over varying amounts of time depending on
880 each experiment. Dose response curves were generated with Prism v9.3.1 using a variable
881 slope, four parameter nonlinear regression model. Comparison between treatment groups were
882 done between IC50 values using the sum-of-squares F test. Details for timing and replicates for
883 each experiment are included in their respective figure legends.

884

885 **Antibodies and Western Blotting**

886 Whole cell lysates were prepared from cultured cells using RIPA lysis and extraction buffer
887 (ThermoScientific). Lysates from xenograft tissues were prepared using tissue protein extraction
888 reagent (T-PER) and glass tissue homogenizer. All lysates were prepared on ice and with the
889 addition of Halt protease and phosphatase inhibitor cocktail and EDTA (ThermoFisher). Protein
890 concentration of lysates were quatified with BCA protein assay (Pierce™, ThermoFisher). All
891 lysates were prepared with 4X Licor Loading buffer with 50mM DTT added boiled for 10 minutes
892 prior to gel loading. All western blots were run using PROTEAN TGX precast 4-15% or 4-20%
893 gradient gels (Bio-Rad) and transferred to either 0.2μm or 0.44μm nitrocellulose membranes.
894 Transfer was done for 1.5-2hrs in cold TrisGlycine buffer (Bio-Rad) with 20% methanol prior
895 blocking for 1hr at room temperature in 5% BSA in TBS-T. Primary antibodies were diluted and
896 incubated overnight at 4°C on a rocker. Membranes were washed 3 or 4 times in fresh TBS-T
897 prior a 1 hour room temperature incubation in an appropriate secondary antibody. Membranes
898 were washed 3-4 times in TBS-T, developed with enhanced SuperSignal West Pico Plus or

899 SuperSignal West Fempto (ThermoFisher) and imaged using Li-Cor Odyssey® Fc instrument.
900 Densitometry was performed using LiCor Image Studio™ software. Statistical comparisons
901 using densitometry measurements were done using a one-way ANOVA with Tukey post hoc to
902 control for the experiment-wise error rate.

903 Western Blot Primary Antibodies:

Target	Vendor	Catalog number	Dilution	Type
GAPDH	Cell Signaling	5174S	1:1000	Rabbit polyclonal
H2AX	Thermofisher	MA1-2022	1:1000	Mouse monoclonal
LRRC8A	LifeSpanBio (LSBio)	LS-C179163-100	1:1000	Rabbit polyclonal
LRRC8D	Sino Biological	104245-T32	1:1000	Rabbit polyclonal
NPEPPS	Thermofisher	PA5-83788	1:1000	Rabbit polyclonal

904 Western Blot Secondary Antibodies:

Target	Vendor	Catalog number	Dilution	Type
Goat-anti-Rabbit(HRP)	Abcam	ab97057	1:20,000	Goat polyclonal
Rabbit-anti-Mouse(HRP)	Sigma	A9044-2ML	1:10,000	Rabbit polyclonal

905

906 **Immunoprecipitation**

907 Immunoprecipitation of genetically modified human bladder cancer cell lines was carried out
908 using Protein G Sepharose beads following manufacturer protocol (GE healthcare). Cells were
909 lysed using Pierce IP lysis buffer containing 25 mM Tris HCL pH 7.4, 150mM NaCl, 1% NP-40,
910 1 mM EDTA, 5% glycerol added with phosphatase and protease inhibitor mixture (Roche
911 Applied Sciences). Sepharose beads slurry has been washed three times with the lysis buffer
912 by centrifuging at 3,000 x g for 2 min at 4°C. Then conjugated anti-FLAG antibody was carried
913 out by overnight incubation of the suspended Protein G Sepharose and anti-FLAG monoclonal
914 antibody (Sigma F1804) at 4°C with continuous mixing. After three-time washing with lysis
915 buffer, the mixture was incubated with the lysates at 4°C overnight with gentle mixing on a
916 suitable shaker. Next, the precipitated protein with the bead was washed three times and
917 analyzed using the immunoblotting technique as described[97]. Whole-cell lysate has been used
918 for input or positive control. Anti-FLAG pull down was performed for FLAG non-expressing
919 bladder cancer cell line for negative control. NPEPPS and LRRC8A were probed using Rabbit
920 polyclonal NPEPPS antibody (1:1000; Thermo Scientific), Rabbit IgG polyclonal LRRC8A
921 antibody (1:1000, LSBio) and Rabbit IgG polyclonal LRRC8D antibody (1:1000, SinoBiological).
922
923 Immunoprecipitation of endogenous (unmodified) human bladder cancer cell lines was
924 performed using Thermo Scientific Pierce Classic Magnetic IP/Co-IP Kit with Pierce Protein A/G
925 magnetic beads and Pierce IP lysis buffer as described above. Beads were washed in three
926 times lysis buffer and cells were incubated in 4% paraformaldehyde for 10 minutes to induce
927 crosslinking conditions prior to lysis. Cell lysate was separated by centrifugation and the protein
928 portion was then incubated with 3ug of anti-NPEPPS (Thermo Scientific) or anti-LRRC8A
929 (LSBio) antibody overnight with gentle mixing at 4°C. Precipitated protein was washed and
930 analyzed via Western Blotting as described above, using whole cell lysate and IgG isotype
931 controls.
932

933 Immunoprecipitation Pulldown Antibodies:

Target	Vendor	Catalog number	Amount	Type
FLAG	Millipore Sigma	F1804	1:50	Mouse monoclonal

IgG	Cell Signaling Technology	CST2729	3 ug	Rabbit monoclonal
LRRC8A/SWELL1	Cell Signaling Technology	CST24979S	3 ug	Rabbit polyclonal
LRRC8D	Sino Biological	104245-T32	3 ug	Rabbit polyclonal
NPEPPS	Thermo Scientific	PA5-83788	3 ug	Rabbit polyclonal

934

935 **Cisplatin induced NPEPPS mRNA expression**

936 Total RNA was isolated from cells using Trizol (ThermoFisher) and standard phenol-chloroform
937 based extraction methods. Residual DNA was digested with DNAse I (Life technologies). cDNA
938 synthesis was performed using Superscript II Reverse Transcriptase kit (Life technologies)
939 using random primers. RT-qPCR reactions were performed on a CFX Connect Real-Time PCR
940 Detection System thermocycler (Bio-Rad) using TaqMan™ gene expression assays for
941 NPEPPS and HMBS as a housekeeping gene (ThermoFisher) in combination with
942 SensiFAST™ Probe No-ROX Kit (Bioline, Toronto, Canada). Expression data was calculated
943 using $2^{-\Delta\Delta Ct}$. All cell line experiments were performed in triplicate from independently grown
944 cells. Comparisons at the indicated dose of cisplatin were made to the control treatment (0μM
945 cisplatin) using a t-test.

946

947 **siRNA-mediated knockdown experiments**

948 NPEPPS and non-targeting siRNA SMARTpools were purchased from Horizon Discovery and
949 resuspended in Dharmacon 5X siRNA Buffer. Transfections were performed using
950 Lipofectamine RNAiMax (ThermoFisher) transfection reagent according to the manufacturer's
951 specifications. Briefly, cells were grown to ~60% confluence in 6-well plates prior to being
952 transfected and allowed to incubate overnight. The following day cells were trypsinized and
953 replated into 96-well plates at 1000-2000 cells per well and allowed to attach overnight. Cells
954 from the initial transfection were also replated into 6-well plates to collect protein and RNA to
955 confirm knockdown. The following day, cells were treated using their previously established
956 resistance doses of gemcitabine, cisplatin, or gemcitabine plus cisplatin (**Table S1**), and their
957 relative growth rates were measured on the IncuCyte ZOOM (Essen Bioscience) over time. For
958 the CyTOF experiments, cells were grown in siRNA SMARTpools for 72 hours before beginning
959 cisplatin treatment.

960

961 **shRNA-mediated knockdown experiments**

962 Lentiviral production and transduction were carried out by the University of Colorado Cancer
963 Center Functional Genomics Shared Resources. Plasmids from The RNAi Consortium (TRC)
964 collection (TRC construct numbers TRCN0000073838, TRCN0000073839 and
965 TRCN0000073840) were used for targeting NPEPPS were selected based on predicted
966 knockdown efficiency; non-targeting controls used were SHC002 and SHC016. 2μg of target
967 shRNA construct and 2μg of 3:1 ratio of psPAX2 (Addgene) and pMD2.G (Addgene) were
968 transfected into HEK293FT cells using 2 μg of Polyethylenimine (Polysciences). Lentiviral
969 particle containing media was filtered using 0.45μm cellulose acetate syringe filter and used for
970 transduction. Puromycin selection was performed at doses used for CRISPR library screening
971 or in some cases, cells were re-selected with higher doses of puromycin (10μg/mL), in order to
972 ensure complete elimination of non-transduced cells. Selected cells were frozen at early
973 passage and early passage cells were used for all experiments.

974

975 **CRISPR knockout of NPEPPS and overexpression addbacks**

976 Bladder cancer cell lines were transduced with a lentiviral inducible Cas9-GFP vector and
977 selected with neomycin (pIndCas9-GFP). Subsequently, these cells were transduced with
978 lentiGUIDE-puro vector containing the NPEPPS-targeting gRNA.

979 The pIndCas9-GFP plasmid was generated by first cloning Cas9-NLS-T2A-GFP from PX458
980 (Addgene plasmid #48138) into pENTR4 (Invitrogen), then shuttling Cas9-NLS-T2A-GFP into
981 pInducer20 (Plasmid #44012) using an LR reaction. The plasmid sequence was verified by
982 complete plasmid sequencing at the Massachusetts General Hospital Center for Computational
983 and Integrative Biology (CCIB) DNA core.

984 CRISPR plasmids targeting NPEPPS were generated by annealing synthetic oligos (NPEPPS
985 F, caccGCAAAGGCTGTAGTTGATGG; NPEPPS R, aaacCCATCAACTACAGCCTTTG) and
986 ligating them into BsmBI-cut lentiGUIDE-puro (Addgene vector #52963) vector; the cloning
987 protocol was adapted from Sanjana, et al.[98]

988 The lentiviral vectors for expressing NPEPPS were cloned by VectorBuilder. Human NPEPPS
989 (NM_006310.4) with a 3' 3xFLAG-tag was cloned under the control of CMV in a lentiviral vector
990 expressing a blasticidin-resistant cassette. An empty vector was used as control.

991 All lentiviral particles were generated in HEK293FT transfected with 2µg of transfer plasmid,
992 2µg of packaging vector mix (PVM) consisting of 2:1 ratio of psPAX2 (Addgene Plasmid
993 #12260) and pMD2.G (Addgene Plasmid #12259) and 12µg Polyethyleneimine (PEI,
994 Polyscience Inc.). All stable cell lines were generated by transduction with 2ml LV and 4µl of
995 polybrene (8mg/ml).

996

997 **Intracellular cisplatin measurements using CyTOF**

998 Cell lines were cultured for several passages in IMDM + 10% FBS. Prior to experiment, cells
999 were cultured in IMDM10 to be 50-80% confluence overnight and then treated the next day with
1000 varying concentrations of cisplatin or PBS as indicated and then dissociated after 4 hours of
1001 treatment. For dissociation, cells were washed twice with room temperature PBS and then
1002 incubated with PBS + 0.05% Trypsin-EDTA for 10-15 minutes. Cells were neutralized with
1003 IMDM10 and then fully dissociated into single-cell suspension by gentle pipetting. After
1004 dissociation, cells were counted by Trypan blue staining and then placed in separate tubes at 3
1005 x 10^5 cells. Individual samples were then fixed, permeabilized, and labeled using unique
1006 barcodes using the Cell-ID 20-plex Pd Barcoding kit (Fluidigm) according to the manufacturer's
1007 protocol. Barcoded samples were pooled across cell line conditions and cisplatin concentration,
1008 incubated with Cell-ID Intercalator-Ir, mixed with equilibration beads, and acquired on a Helios
1009 mass cytometer (Fluidigm). Post-acquisition data were normalized to equilibration beads and
1010 debarcoded, using the bead-normalization and single-cell-debarcoder packages from the Nolan
1011 Laboratory GitHub page (https://github.com/nolanlab). Relative cisplatin intensity (defined by
1012 ^{195}Platinum isotopic mass intensity) was analyzed among nucleated ^{191}Iridium+ ^{193}Iridium+
1013 events defined by Boolean gating within FlowJo 10.7.1.
1014

1015 **Whole Genome CRISPR Screening**

1016 ***Plasmid library expansion and quality control***

1017 Whole genome CRISPR Screening was performed using the Human CRISPR Knockout Pooled
1018 Library (Brunello) - 1 vector system (Addgene and a gift from John Doench to the Functional

1019 Genomics Facility at the University of Colorado Anschutz Medical Campus)[26]. Two distinct
1020 plasmid expansions were performed. And the library distribution was assessed using next
1021 generation sequencing to determine the impact on overall library was modest following re-
1022 expansion. Library width was calculated as previously described[99,100] by dividing the 10th
1023 percentile of the library distribution by the 90th percentile using the log2 average expression of
1024 all sgRNAs in the library and found to be 6.7 and 7.13 for batch 1 and 2 respectively. All quality
1025 control metrics for each sample are reported in **Table S15**. Different screening parameters were
1026 used based on the cell line screened these are summarized in **Table S4.**

1027 ***Lentivirus Production and Titration***

1028 For the two plasmid batches, two distinct protocols for lentivirus production were utilized. The
1029 first batch was generated by using Polyethylenimine, linear (PEI; Polysciences) and was used
1030 for the T24-GemCis and TCCSUP-GemCis screens. The second used lipofectamine 3000 and
1031 was applied for the 253J-GemCis, KU1919-GemCis, and 5637-GemCis screens. For the first
1032 batch, 293FT cells were seeded at a density of 36,800 cells/cm^2 into a 4-layer CELLdisc
1033 (Greiner) using DMEM + 10% FBS along with antibiotic and antimycotic solution. Transfection
1034 mix consisting 47.6μg pMD2G (Addgene), 95.2μg of psPAX2 (Addgene), and 190.5μg of
1035 Brunello Whole genome knockout library (Addgene) was mixed with 448μl PEI (1 mg/mL) and
1036 3mL OptiMEM, vortexed for 30 seconds and allowed to incubate at room temperature for 20
1037 minutes. Fresh media containing transfection mix were added to the CELLdisc using up to
1038 270mL of media. The next day media was changed for 280mL fresh media followed by a 48-
1039 hour incubation. After this 48-hour incubation the viral supernatant was harvested and filtered
1040 through a cellulose acetate filter system (ThermoScientific) and frozen at -80°C.

1041 The first method had low functional virus titer, so we implemented a different virus production
1042 method for subsequent screens. In the second batch of virus production, we utilized
1043 lipofectamine 3000 instead of PEI, eliminated use of multilayer flasks and centrifuged to remove
1044 debris as opposed to filtering. Briefly, 293FT cells were plated in T225 flasks to be 80%
1045 confluent after 24hrs. 2hrs before transfection, media was changed and 40mL of fresh media
1046 was used per T225 flask. The lipofectamine 3000 protocol was followed according to
1047 manufacturer's instructions and scaled based on the volume of virus being prepared. For each
1048 T225 flask 2mLOptiMEM was mixed with 40μg Brunello whole genome library plasmid, 30μg of
1049 psPAX2 and 20μg of pMD2.G and 180μl of P3000. This mix was added to a tube containing
1050 2mL OptiMEM and 128μl Lipofectamine 3000, which was scaled according to the number of
1051 T225 flasks being prepared. Transfection mix was mixed thoroughly by pipetting up and down
1052 slowly, and allowed to incubate at room temperature for 15 minutes. Transfection mix was then
1053 added dropwise to the plates of 293FT cells with gentle swirling and incubated overnight
1054 (~16hr). The following morning, the media was changed and 60mL of fresh media was added to
1055 each T225 flask. This was allowed to incubate overnight and replaced the following morning.
1056 This first lentiviral supernatant was stored at 4°C to be pooled with a subsequent 48 hour
1057 collection. Upon collection, viral supernatants had 1M HEPES added at 1%. Following the
1058 second virus collection, supernatants were pooled and centrifuged at 1250rpm for 5 minutes to
1059 pellet debris. Lentivirus was stored in polypropylene tubes as polystyrene is known to bind
1060 lentivirus, and all tubes were flash frozen in liquid nitrogen and stored at -80°C. Despite the
1061 changes to the lentiviral production protocols, functional lentiviral titers were not improved using
1062 these changes to the methodology, but feel it is worth noting these changes in protocol to
1063 account for any possible variability associated with this change.

1064 Lentivirus was titered functionally based on protocols adapted from the Broad Institute's Genetic
1065 Perturbation Platform's public web portal (https://portals.broadinstitute.org/gpp/public/).

1066

1067 ***Screening Parameter Optimization***

1068 All screening parameters for each cell line including cell polybrene and puromycin sensitivity,
1069 screening coverage, technical and biological replicates performed, and gemcitabine and
1070 cisplatin treatment concentrations are reported in **Table S4.**

1071 ***DNA Isolation***

1072 Cell pellets of 2e7 were snap frozen in liquid nitrogen in 1.5mL tubes and stored at -80 prior to
1073 extraction. When possible, at least 8e7 cell were used for 4 separate genomic DNA isolation
1074 which were pooled to account for any variation with pellet size. DNA isolation was performed
1075 using the Puregene cell and tissue kit (Qiagen) with the addition of RNase A Solution (Qiagen)
1076 according to the manufacturer's instructions. DNA concentration was measured in quadruplicate
1077 using either a nanodrop spectrophotometer (Thermo), Qubit® dsDNA assay (Life
1078 Technologies), and the average DNA content per cell was determined.

1079 ***Library preparation***

1080 The minimum number of cell equivalents of gDNA to maintain equal coverage was used for
1081 library preparation. In all screens, the minimum coverage based on cell number was multiplied
1082 by the average gDNA content per cell for each individual cell line to determine the minimum
1083 number for 10μg PCR reactions needed to maintain coverage. A minimum coverage of 500-fold
1084 per sgRNA in the library was targeted for each independent sample or replicate but this was
1085 increased in some cases where screening was carried out with greater depth (see **Table S4** for
1086 coverage and replicate information).

1087 Library preparation was performed using primers sequences designed by the Broad Institute's
1088 Genetic Perturbation Platform (https://portals.broadinstitute.org/gpp/public/) and utilized a pool
1089 of eight P5 primers with to introduce a stagger in reads associated with each library and sample
1090 specific P7 primer that contained a unique sample index sequence for each timepoint, replicate,
1091 or treatment condition to be sequenced in the same pool (**Table S12**). All library preparation
1092 primers were resuspended at 100μM.

1093 Each library preparation PCR reaction contained the following components: 1μl Herculase II
1094 Fusion Enzyme (Agilent), 2.5μl Deoxynucleotide (dNTP) Solution Mix (New England Biolabs),
1095 0.5μl P5 primer pool, 0.5μl P7 index primer, 20μl 5X Reaction Buffer (Agilent), 10μg of gDNA
1096 and nuclease-free water to bring the total reaction volume to 100μl. Samples underwent 23
1097 cycles of thermal cycling followed by a quality assessment by electrophoresis on 2% agarose
1098 gel to ensure consistent library amplification across multiple wells and samples for each plate.

1099 Each unique library had 10μl pooled from all PCR reactions performed on that unique sample
1100 and mixed thoroughly. 50-100μl of the pooled library preparation reactions was used to perform
1101 magnetic bead-based purification and elimination of any residual free primer using a 0.8X ratio
1102 SPRIselect beads (Beckman Coulter) according to the manufacturer's instructions. Libraries
1103 were then assessed for appropriate amplicon size and complete elimination of free primer peaks
1104 using the High Sensitivity ScreenTape Assay on the Tape Station2200 (Agilent) and quantified
1105 using the qPCR-based quantification in order to ensure only NGS-compatible amplicon was
1106 quantified using the Library Quant ROX Low Kit (Kapa Biosystems) on a QuantStudio™ 6
1107 Realtime PCR System (ThermoFisher). Following qPCR quantification, all libraries were
1108 normalized to a standard concentration (typically 20-40nM) depending on the lowest
1109 concentration library to be pooled, and then requantified by qPCR to ensure all samples were
1110 within ~10-20% of the pool mean target concentration. After confirming accurate library
1111 quantification and normalization, samples were pooled at an equimolar ratio and submitted for

1112 sequencing. Libraries were sequenced on the NovaSeq 6000 instrument (Illumina) (150bp,
1113 paired-end) at the University of Colorado Cancer Center Genomics Shared Resource.

1114 ***CRISPR screening bioinformatic pipeline and analysis***

1115 sgRNA counts were extracted directly from R1 raw sequence reads using a custom perl script
1116 that uses regular expression string matching to exactly match sgRNA sequence flanked by 10
1117 bases of vector sequence. The vector sequence was allowed to have one error before and after
1118 the sgRNA sequence. sgRNAs were tabulated for each sample based on the sgRNA sequence
1119 (**Table S16**). The sgRNA IDs of the Brunello library were updated to current HGNC gene names
1120 using the Total Approved Symbols download from HGNC, accessed on 9/1/2020
1121 (https://www.genenames.org/download/statistics-and-files/). Transcript IDs were matched when
1122 possible and when matches were not found, past symbols and aliases were updated to current
1123 names. Finally, 5 sgRNAs with missing updated gene names were manually curated using
1124 literature searches. Library distribution was calculated using the caRpools R package[101] (**Table**
1125 **S12)**. The DESeq2 R package[102] was used to calculate differential abundance of genes (**Table**
1126 **S5**). Gene counts were generated using the sum of counts for sgRNAs of the same gene.
1127 Synthetic lethality compared GemCis day 19 and GemCis day 25 vs. PBS day 19 and PBS day
1128 25 with the day as a covariate. In the comparison integrating all cell lines, cell line was
1129 additionally modeled as a covariate. Gene essentiality was calculated by comparing PBS day 25
1130 to PBS day 0 and in the integrated all cell lines comparison; cell line was modeled as a
1131 covariate. Common synthetic lethal genes were defined as being statistically significantly
1132 differentially lost (FDR < 0.05 and Log2 FC < 0) in each of the 5 cell lines. Gene set enrichment
1133 analysis (GSEA) was performed using the fgsea R package run with 10000 permutations[71] with
1134 the KEGG and Reactome gene sets from MSigDB[72]. Heatmaps were generated with the
1135 ComplexHeatmap R package following z-score transformation[74]. Other plots were generated
1136 using the ggplot2 R package.

1137 **Xenograft experiment**

1138 Six-week-old, female NU/J mice (Jackson Labs) were allowed to acclimate for at least one week
1139 prior to initiating any experiments. Mice had free access to food and water in pathogen-free
1140 housing and cared for in accordance NIH guidelines and all experiments were performed under
1141 protocols approved by the University of Colorado Denver Institutional Animal Care and Use
1142 Committee (IACUC).

1143 For KU1919-GC xenografts, cells that had been stably transduced with non-targeting control
1144 (shCtrl1, SHC002) and NPEPPS (shN39, TRCN0000073839) shRNA constructs. Mice were
1145 divided into groups of 22 and 23 for the non-targeting control and NPEPPS shRNA constructs
1146 respectively. Mice were injected with 4e6 cells in phenol red- and serum-free RPMI mixed with
1147 equal volume Matrigel Matrix (Corning) to total 100μl volume. Tumors were allowed to engraft
1148 for 9 days following injection and mice were randomized based on tumor volume within each
1149 shRNA condition into groups of 11 or 12 to be treated with combination gemcitabine plus
1150 cisplatin or DPBS. Treatment was initiated 13 days post-inoculation with dosing adjusted based
1151 on individual mouse weight.

1152 Cisplatin (Sigma) and gemcitabine hydrochloride (BOC Sciences) were both resuspended in
1153 0.9% saline and stored protected from light at -80°C as individual aliquots. Prior to treatment
1154 fresh aliquots of gemcitabine and cisplatin were thawed and diluted to their final concentration
1155 with 1X DPBS (Gibco). Mice were treated three times weekly on a Monday, Wednesday and
1156 Friday schedule for four weeks total. All mice in the gemcitabine plus cisplatin treated groups
1157 were given 50mg/kg gemcitabine and 2mg/kg cisplatin that were mixed and administered as a
1158 single intraperitoneal injection, while control mice were administered an equivalent volume of
1159 DPBS.

Mouse health was monitored daily and all tumor volume measurements and weights were measured 3x weekly schedule. Tumor volume was calculated using the formula (L x W^2)/2, for which L *is* the length of the long axis and W is the width of the axis perpendicular to the long axis measurement. All measurements were performed using digital calipers. Animal were humanely euthanized with CO_2 followed by cervical dislocation when tumors reached a predetermined endpoint of 2cm^3 or when weight loss exceeded 15% body weight. Mice that were removed from study due to weight loss were censored in the survival analyses.

Linear mixed-effects model of tumor growth

Linear mixed-effects models were used to model longitudinal observations of xenograft tumor growth volumes normalized by their corresponding baseline volume. Mixed-effects models from the R-package *lme4*[103] and Satterthwaite's approximation for degrees of freedom for the fixed effects from *lmerTest*[104] were used for model fitting and inspection in the R statistical software (4.0.3). Volume changes compared to baseline were log_2-transformed. The final model was structured as:

$$log_2\left(\frac{y_{i,t}}{y_{i,:}}\right) = \beta_0 + \beta_1 x_{i,t} + \beta_2 x_{i,t}^2 + \beta_3 x_{i,t} KD_i + \beta_4 x_{i,t} GC_i + \beta_5 x_{i,t} KD_i\, GC_i + \gamma_{0,i} + \gamma_{1,i} x_{i,t} + \varepsilon_{i,t}$$

where β is the fixed effects capturing population-level trends, γ is the normally distributed random effects capturing individual-level variation, ε is the i.i.d. normally distributed residual term, i is the unique individual identifier, t notes the time points, $x_{i,t} \in \{2, 4, 5, 7, 9, 11, 14, 16, 18, 21, 23, 25, 28\}$ depicted days since initiating interventions, $y_{i,:}$ is tumor volume at baseline prior to treatments upon randomization, and $y_{i,t}$ were the observed tumor volumes over the treatment period measured in mm^3. The model was fit using Restricted Maximum Likelihood and built iteratively until the underlying model assumptions and model convergence criteria were met. To this end, a quadratic growth term (β_2) was added on top of the linear growth term (β_1) and intercept (β_0), allowing slightly non-linear relative growth patterns to be captured by the otherwise linear model. Binary indicators $KD_i \in \{0,1\}$ and $GC_i \in \{0,1\}$ were used to model knockdown of NPEPPS, GemCis treatment, or the combination. The corresponding model terms were captured in β_3, β_4 and β_5, respectively. Finally, the model allows for individual-specific random effects for intercept ($\gamma_{0,i}$) and linear growth slope ($\gamma_{1,i}$). Shapiro-Wilk test was used to examine the underlying normality assumption for $\gamma_{0,i}$ and $\gamma_{1,i}$ with p=0.1373 and p=8901, respectively, indicating that these random effects followed underlying assumptions of normality. After inspection of the residual plots (**Figure S9B**), this final model was deemed suitable for population-level statistical inference via the fixed effects. This population-level model fits are visualized in **Figure S9A**. These population-level estimates are as follows:

Fixed effect	**Estimate**	**Std. error**	**df**	**t**	***p*-val**
β_0 (intercept)	0.05054	0.08422	54.28	0.600	0.55091
β_1 (linear slope)	0.1236	0.01493	65.52	8.276	8.92e-12 ***
β_2 (quadratic slope)	0.00308	0.0002242	389	13.740	< 2e-16 ***
β_3 (knockdown)	-0.0605	0.01821	44.97	-3.322	0.00178 **
β_4 (GC)	-0.1063	0.01821	44.97	-5.837	5.49e-07 ***
β_5 (knockdown + GC)	-0.1233	0.01791	45.28	-6.884	1.47e-08 ***

1197 **Survival analyses from TCGA**

1198 Copy number and gene expression data for patients with muscle-invasive bladder cancer in the
1199 TCGA cohort (PanCancer Atlas) were downloaded from cBioPortal[105,106]. Patient survival and
1200 platinum-based treatment annotation was from our previous work[18]. Patients were separated
1201 into treatment groups, platinum-based treatment (n = 98) or unrecorded treatment (n = 204),
1202 and then stratified based on copy number gain or amplification, or mRNA upregulation (z-score
1203 > 1) of LRRC8A or LRRC8D. For NPEPPS, patients were stratified on median gene expression.
1204 The Logrank test was used to test the difference in overall survival between the stratified patient
1205 groups.

1206

1207 ***Data availability***

1208 The mass spectrometry proteomics data have been deposited to the ProteomeXchange
1209 Consortium via the PRIDE[107] partner repository with the dataset identifier PXD024742. The
1210 whole exome sequencing data have been deposited in the BioProject database with project
1211 identifier PRJNA714778. The RNA sequencing data have been deposited in the GEO database
1212 with dataset identifier (GSE171537). The CRISPR screen sequencing data have been
1213 deposited in the GEO database with dataset identifier (submission in progress). The copy
1214 number data have been deposited in the ArrayExpress database with identified (E-MTAB-
1215 10353).
1216
1217 *Reviewer Login Information*
1218 **PRIDE**
1219 Username: reviewer_pxd024742@ebi.ac.uk
1220 Password: n70IwGNc
1221
1222 **SRA**
1223 https://dataview.ncbi.nlm.nih.gov/object/PRJNA714778?reviewer=50g24ej0558qj2dpr9v6pekgvl
1224
1225 **GEO (RNAseq)**
1226 https://www.ncbi.nlm.nih.gov/geo/query/acc.cgi?acc=GSE171537
1227 token: avkdyoiixnettod
1228
1229 **ArrayExpress**
1230 Username: Reviewer_E-MTAB-10353
1231 Password: u3MpsspP
1232

Acknowledgements

We would like to thank Megan Tu, Colin Sempeck, Ana Chauca-Diaz, Jason Duex, and Charles Owens for their help throughout this project. We would also like to thank Dania Manalo-Mae and the Cedars-Sinai Proteomics and Metabolomics Core Facility for the technical handling of the proteomic experiments. This work was generously supported by the Anschutz Foundation to J.C.C., CA180175 to D.T., CA268055 to D.T. and J.C.C., FICAN Cancer Researcher by the Finnish Cancer Institute to T.D.L., Erasmus MC mRACE grant 111296 to T.Z., Erasmus MC fellowship project 107088 to T.Z., and training grants GM007635 and GM008497 supported R.T.J. This work utilized the Functional Genomics Facility, Biostatistics and Bioinformatics Shared Resource, Genomics Shared Resource, and Flow Cytometry Shared Resource supported by CA046934.

Author Contributions

Conceptualization: R.T.J., T.Z., D.T., J.C.C.
Methodology: R.T.J., A.G., S.M., L.E.F., H.V., A.J., C.B.T., C.D., T.D.L., E.T.C., S.P., T.Z., D.T., J.C.C.
Software: A.G., T.D.L., M.J., R.L., J.C.C.
Validation: R.T.J., A.G., S.M., L.E.L., M.S., A.J., C.B.T., M.V.O., C.D., N.X., S.A., T.Z.
Formal Analysis: R.T.J., A.G., L.E.F., M.S., H.V., T.D.L., M.V.O., C.D., N.X., M.J., E.T.C., S.P., T.Z., D.T., J.C.C.
Investigation: R.T.J., S.M., L.E.F., M.S., H.V., A.J., C.B.T., M.V.O., C.D., N.X., S.A., E.T.C., S.P., T.Z., J.C.C.
Resources: A.J., C.B.T., E.T.C., R.L., T.Z.
Data Curation: R.T.J., A.G., A.J., T.D.L., M.J., R.L., J.C.C.
Writing – Original Draft: R.T.J., A.G., D.T., J.C.C.
Writing – Review & Editing: R.T.J., A.G., S.M., L.E.F., M.S., H.V., M.V.O., C.D., M.J., T.D.L., E.T.C., S.P., T.Z., D.T., J.C.C.
Visualization: R.T.J., A.G., M.S., L.E.F., M.V.O., N.X., T.D.L., E.T.C., T.Z., D.T., J.C.C.
Supervision: R.L., D.T., T.Z., J.C.C.
Project Administration: D.T., J.C.C.
Funding Acquisition: D.T., J.C.C.

Competing Interests Statement

A provisional patent 63/153,519 has been filed on the subject matter of this work. J.C.C. is co-founder of PrecisionProfile and OncoRX Insight. All other authors declare no competing interests.

1272 **References**

1273 1. Dilruba, S. & Kalayda, G. V. Platinum-based drugs: past, present and future. *Cancer*
1274 *Chemother. Pharmacol.* **77**, 1103–1124 (2016).
1275 2. Rottenberg, S., Disler, C. & Perego, P. The rediscovery of platinum-based cancer therapy.
1276 *Nat. Rev. Cancer* **21**, 37–50 (2021).
1277 3. Galluzzi, L. *et al.* Molecular mechanisms of cisplatin resistance. *Oncogene* **31**, 1869–1883
1278 (2012).
1279 4. Planells-Cases, R. *et al.* Subunit composition of VRAC channels determines substrate
1280 specificity and cellular resistance to Pt-based anti-cancer drugs. *EMBO J.* **34**, 2993–3008
1281 (2015).
1282 5. Bray, F. *et al.* Global cancer statistics 2018: GLOBOCAN estimates of incidence and mortality
1283 worldwide for 36 cancers in 185 countries. *CA. Cancer J. Clin.* **68**, 394–424 (2018).
1284 6. Galsky, M. D. *et al.* Real-World Effectiveness of Chemotherapy in Elderly Patients With
1285 Metastatic Bladder Cancer in the United States. *Bladder Cancer Amst. Neth.* **4**, 227–238
1286 (2018).
1287 7. Patel, V. G., Oh, W. K. & Galsky, M. D. Treatment of muscle-invasive and advanced bladder
1288 cancer in 2020. *CA. Cancer J. Clin.* (2020) doi:10.3322/caac.21631.
1289 8. Galsky, M. D. *et al.* Atezolizumab with or without chemotherapy in metastatic urothelial
1290 cancer (IMvigor130): a multicentre, randomised, placebo-controlled phase 3 trial. *Lancet*
1291 *Lond. Engl.* **395**, 1547–1557 (2020).
1292 9. Nadal, R. & Bellmunt, J. Management of metastatic bladder cancer. *Cancer Treat. Rev.* **76**,
1293 10–21 (2019).

1294 10. Balar, A. V. *et al.* Atezolizumab as first-line treatment in cisplatin-ineligible patients with
1295 locally advanced and metastatic urothelial carcinoma: a single-arm, multicentre, phase 2
1296 trial. *Lancet Lond. Engl.* **389**, 67–76 (2017).
1297 11. Grossman, H. B. *et al.* Neoadjuvant Chemotherapy plus Cystectomy Compared with
1298 Cystectomy Alone for Locally Advanced Bladder Cancer. *N. Engl. J. Med.* **349**, 859–866
1299 (2003).
1300 12. Vale, C. L. Neoadjuvant Chemotherapy in Invasive Bladder Cancer: Update of a Systematic
1301 Review and Meta-Analysis of Individual Patient Data: Advanced Bladder Cancer (ABC)
1302 Meta-analysis Collaboration. *Eur. Urol.* **48**, 202–206 (2005).
1303 13. Witjes, J. A. *et al.* European Association of Urology Guidelines on Muscle-invasive and
1304 Metastatic Bladder Cancer: Summary of the 2020 Guidelines. *Eur. Urol.* (2020)
1305 doi:10.1016/j.eururo.2020.03.055.
1306 14. Cowley, G. S. *et al.* Parallel genome-scale loss of function screens in 216 cancer cell lines for
1307 the identification of context-specific genetic dependencies. *Sci. Data* **1**, 140035 (2014).
1308 15. McDonald, E. R. *et al.* Project DRIVE: A Compendium of Cancer Dependencies and Synthetic
1309 Lethal Relationships Uncovered by Large-Scale, Deep RNAi Screening. *Cell* **170**, 577-
1310 592.e10 (2017).
1311 16. Tsherniak, A. *et al.* Defining a Cancer Dependency Map. *Cell* **170**, 564-576.e16 (2017).
1312 17. Behan, F. M. *et al.* Prioritization of cancer therapeutic targets using CRISPR–Cas9 screens.
1313 *Nature* **568**, 511–516 (2019).

1314 18. Goodspeed, A., Jean, A. & Costello, J. C. A Whole-genome CRISPR Screen Identifies a Role of
1315 MSH2 in Cisplatin-mediated Cell Death in Muscle-invasive Bladder Cancer. *Eur. Urol.* **75**,
1316 242–250 (2019).
1317 19. Huang, A., Garraway, L. A., Ashworth, A. & Weber, B. Synthetic lethality as an engine for
1318 cancer drug target discovery. *Nat. Rev. Drug Discov.* **19**, 23–38 (2020).
1319 20. Jost, M. & Weissman, J. S. CRISPR Approaches to Small Molecule Target Identification. *ACS*
1320 *Chem. Biol.* **13**, 366–375 (2018).
1321 21. Olivieri, M. *et al.* A Genetic Map of the Response to DNA Damage in Human Cells. *Cell* **182**,
1322 481-496.e21 (2020).
1323 22. Vallo, S. *et al.* Drug-Resistant Urothelial Cancer Cell Lines Display Diverse Sensitivity Profiles
1324 to Potential Second-Line Therapeutics. *Transl. Oncol.* **8**, 210–216 (2015).
1325 23. Vallo, S. *et al.* Resistance to nanoparticle albumin-bound paclitaxel is mediated by ABCB1 in
1326 urothelial cancer cells. *Oncol. Lett.* **13**, 4085–4092 (2017).
1327 24. Robertson, A. G. *et al.* Comprehensive Molecular Characterization of Muscle-Invasive
1328 Bladder Cancer. *Cell* **171**, 540-556.e25 (2017).
1329 25. Landrum, M. J. *et al.* ClinVar: improving access to variant interpretations and supporting
1330 evidence. *Nucleic Acids Res.* **46**, D1062–D1067 (2018).
1331 26. Doench, J. G. *et al.* Optimized sgRNA design to maximize activity and minimize off-target
1332 effects of CRISPR-Cas9. *Nat. Biotechnol.* **34**, 184–191 (2016).
1333 27. Korotkevich, G., Sukhov, V. & Sergushichev, A. Fast gene set enrichment analysis. *bioRxiv*
1334 060012 (2019) doi:10.1101/060012.

1335 28. Drayton, R. M. & Catto, J. W. Molecular mechanisms of cisplatin resistance in bladder
1336 cancer. *Expert Rev. Anticancer Ther.* **12**, 271–281 (2012).
1337 29. Huang, D. *et al.* A highly annotated database of genes associated with platinum resistance
1338 in cancer. *Oncogene* **40**, 6395–6405 (2021).
1339 30. Dempster, J. M. *et al.* Gene expression has more power for predicting in vitro cancer cell
1340 vulnerabilities than genomics. *bioRxiv* 2020.02.21.959627 (2020)
1341 doi:10.1101/2020.02.21.959627.
1342 31. Bepler, G. *et al.* RRM1 modulated in vitro and in vivo efficacy of gemcitabine and platinum
1343 in non-small-cell lung cancer. *J. Clin. Oncol. Off. J. Am. Soc. Clin. Oncol.* **24**, 4731–4737
1344 (2006).
1345 32. Bergman, A. M. *et al.* In vivo induction of resistance to gemcitabine results in increased
1346 expression of ribonucleotide reductase subunit M1 as the major determinant. *Cancer Res.*
1347 **65**, 9510–9516 (2005).
1348 33. Jordheim, L. P., Sève, P., Trédan, O. & Dumontet, C. The ribonucleotide reductase large
1349 subunit (RRM1) as a predictive factor in patients with cancer. *Lancet Oncol.* **12**, 693–702
1350 (2011).
1351 34. Constam, D. B. *et al.* Puromycin-sensitive aminopeptidase. Sequence analysis, expression,
1352 and functional characterization. *J. Biol. Chem.* **270**, 26931–26939 (1995).
1353 35. Saric, T., Graef, C. I. & Goldberg, A. L. Pathway for degradation of peptides generated by
1354 proteasomes: a key role for thimet oligopeptidase and other metallopeptidases. *J. Biol.*
1355 *Chem.* **279**, 46723–46732 (2004).

1356 36. Towne, C. F. *et al.* Puromycin-Sensitive Aminopeptidase Limits MHC Class I Presentation in
1357 Dendritic Cells but Does Not Affect CD8 T Cell Responses during Viral Infections. *J.*
1358 *Immunol.* **180**, 1704–1712 (2008).
1359 37. Menzies, F. M. *et al.* Puromycin-sensitive aminopeptidase protects against aggregation-
1360 prone proteins via autophagy. *Hum. Mol. Genet.* **19**, 4573–4586 (2010).
1361 38. Huttlin, E. L. *et al.* Dual Proteome-scale Networks Reveal Cell-specific Remodeling of the
1362 Human Interactome. *bioRxiv* 2020.01.19.905109 (2020) doi:10.1101/2020.01.19.905109.
1363 39. Qiu, Z. *et al.* SWELL1, a plasma membrane protein, is an essential component of volume-
1364 regulated anion channel. *Cell* **157**, 447–458 (2014).
1365 40. Thompson, M. W. & Hersh, L. B. Analysis of conserved residues of the human puromycin-
1366 sensitive aminopeptidase. *Peptides* **24**, 1359–1365 (2003).
1367 41. Voss, F. K. *et al.* Identification of LRRC8 heteromers as an essential component of the
1368 volume-regulated anion channel VRAC. *Science* **344**, 634–638 (2014).
1369 42. Sørensen, B. H., Thorsteinsdottir, U. A. & Lambert, I. H. Acquired cisplatin resistance in
1370 human ovarian A2780 cancer cells correlates with shift in taurine homeostasis and ability
1371 to volume regulate. *Am. J. Physiol.-Cell Physiol.* **307**, C1071–C1080 (2014).
1372 43. Sørensen, B. H., Nielsen, D., Thorsteinsdottir, U. A., Hoffmann, E. K. & Lambert, I. H.
1373 Downregulation of LRRC8A protects human ovarian and alveolar carcinoma cells against
1374 Cisplatin-induced expression of p53, MDM2, p21Waf1/Cip1, and Caspase-9/-3 activation.
1375 *Am. J. Physiol.-Cell Physiol.* **310**, C857–C873 (2016).

1376 44. Sørensen, B. H., Dam, C. S., Stürup, S. & Lambert, I. H. Dual role of LRRC8A-containing
1377 transporters on cisplatin resistance in human ovarian cancer cells. *J. Inorg. Biochem.* **160**,
1378 287–295 (2016).
1379 45. Kasuya, G. *et al.* Cryo-EM structures of the human volume-regulated anion channel LRRC8.
1380 *Nat. Struct. Mol. Biol.* **25**, 797–804 (2018).
1381 46. Syeda, R. *et al.* LRRC8 Proteins Form Volume-Regulated Anion Channels that Sense Ionic
1382 Strength. *Cell* **164**, 499–511 (2016).
1383 47. Jackson, P. S. & Strange, K. Volume-sensitive anion channels mediate swelling-activated
1384 inositol and taurine efflux. *Am. J. Physiol.* **265**, C1489-1500 (1993).
1385 48. Chang, Q. *et al.* Single-cell measurement of the uptake, intratumoral distribution and cell
1386 cycle effects of cisplatin using mass cytometry. *Int. J. Cancer* **136**, 1202–1209 (2015).
1387 49. Karsten, S. L. *et al.* A genomic screen for modifiers of tauopathy identifies puromycin-
1388 sensitive aminopeptidase as an inhibitor of tau-induced neurodegeneration. *Neuron* **51**,
1389 549–560 (2006).
1390 50. Kudo, L. C. *et al.* Puromycin-sensitive aminopeptidase (PSA/NPEPPS) impedes development
1391 of neuropathology in hPSA/TAU(P301L) double-transgenic mice. *Hum. Mol. Genet.* **20**,
1392 1820–1833 (2011).
1393 51. Schönlein, C., Löffler, J. & Huber, G. Purification and characterization of a novel
1394 metalloprotease from human brain with the ability to cleave substrates derived from the
1395 N-terminus of beta-amyloid protein. *Biochem. Biophys. Res. Commun.* **201**, 45–53 (1994).
1396 52. Yanagi, K. *et al.* Involvement of puromycin-sensitive aminopeptidase in proteolysis of tau
1397 protein in cultured cells, and attenuated proteolysis of frontotemporal dementia and

1398 parkinsonism linked to chromosome 17 (FTDP-17) mutant tau. *Psychogeriatrics* **9**, 157–166
1399 (2009).
1400 53. Karczewski, K. J. *et al.* The mutational constraint spectrum quantified from variation in
1401 141,456 humans. *Nature* **581**, 434–443 (2020).
1402 54. Uhlen, M. *et al.* A pathology atlas of the human cancer transcriptome. *Science* **357**, (2017).
1403 55. Osada, T. *et al.* Increased anxiety and impaired pain response in puromycin-sensitive
1404 aminopeptidase gene-deficient mice obtained by a mouse gene-trap method. *J. Neurosci.*
1405 *Off. J. Soc. Neurosci.* **19**, 6068–6078 (1999).
1406 56. Pérez-Tomás, R. Multidrug resistance: retrospect and prospects in anti-cancer drug
1407 treatment. *Curr. Med. Chem.* **13**, 1859–1876 (2006).
1408 57. Merino, V., Jiménez-Torres, N. V. & Merino-Sanjuán, M. Relevance of multidrug resistance
1409 proteins on the clinical efficacy of cancer therapy. *Curr. Drug Deliv.* **1**, 203–212 (2004).
1410 58. Bradshaw, D. M. & Arceci, R. J. Clinical relevance of transmembrane drug efflux as a
1411 mechanism of multidrug resistance. *J. Clin. Oncol. Off. J. Am. Soc. Clin. Oncol.* **16**, 3674–
1412 3690 (1998).
1413 59. Hitzerd, S. M., Verbrugge, S. E., Ossenkoppele, G., Jansen, G. & Peters, G. J. Positioning of
1414 aminopeptidase inhibitors in next generation cancer therapy. *Amino Acids* **46**, 793–808
1415 (2014).
1416 60. Krige, D. *et al.* CHR-2797: an antiproliferative aminopeptidase inhibitor that leads to amino
1417 acid deprivation in human leukemic cells. *Cancer Res.* **68**, 6669–6679 (2008).

1418 61. Reid, A. H. M. *et al.* A First-in-Man Phase I and Pharmacokinetic Study on CHR-2797
1419 (Tosedostat), an Inhibitor of M1 Aminopeptidases, in Patients with Advanced Solid
1420 Tumors. *Clin. Cancer Res.* **15**, 4978–4985 (2009).
1421 62. Löwenberg, B. *et al.* Phase I/II clinical study of Tosedostat, an inhibitor of aminopeptidases,
1422 in patients with acute myeloid leukemia and myelodysplasia. *J. Clin. Oncol. Off. J. Am. Soc.*
1423 *Clin. Oncol.* **28**, 4333–4338 (2010).
1424 63. Cortes, J. *et al.* Two dosing regimens of tosedostat in elderly patients with relapsed or
1425 refractory acute myeloid leukaemia (OPAL): a randomised open-label phase 2 study.
1426 *Lancet Oncol.* **14**, 354–362 (2013).
1427 64. van Herpen, C. M. L. *et al.* A Phase Ib dose-escalation study to evaluate safety and
1428 tolerability of the addition of the aminopeptidase inhibitor tosedostat (CHR-2797) to
1429 paclitaxel in patients with advanced solid tumours. *Br. J. Cancer* **103**, 1362–1368 (2010).
1430 65. Mawad, R. *et al.* Phase II study of tosedostat with cytarabine or decitabine in newly
1431 diagnosed older patients with acute myeloid leukaemia or high-risk MDS. *Br. J. Haematol.*
1432 **172**, 238–245 (2016).
1433 66. Compagnone, M., Cifaldi, L. & Fruci, D. Regulation of ERAP1 and ERAP2 genes and their
1434 disfunction in human cancer. *Hum. Immunol.* **80**, 318–324 (2019).
1435 67. Lim, Y. W. *et al.* Germline genetic polymorphisms influence tumor gene expression and
1436 immune cell infiltration. *Proc. Natl. Acad. Sci.* **115**, E11701–E11710 (2018).
1437 68. Dobin, A. *et al.* STAR: ultrafast universal RNA-seq aligner. *Bioinforma. Oxf. Engl.* **29**, 15–21
1438 (2013).

1439 69. Robinson, M. D., McCarthy, D. J. & Smyth, G. K. edgeR: a Bioconductor package for
1440 differential expression analysis of digital gene expression data. *Bioinforma. Oxf. Engl.* **26**,
1441 139–140 (2010).
1442 70. Ritchie, M. E. *et al.* limma powers differential expression analyses for RNA-sequencing and
1443 microarray studies. *Nucleic Acids Res.* **43**, e47 (2015).
1444 71. Sergushichev, A. A. An algorithm for fast preranked gene set enrichment analysis using
1445 cumulative statistic calculation. *bioRxiv* 060012 (2016) doi:10.1101/060012.
1446 72. Liberzon, A. *et al.* Molecular signatures database (MSigDB) 3.0. *Bioinformatics* **27**, 1739–
1447 1740 (2011).
1448 73. Wickham, H. *Ggplot2: elegant graphics for data analysis*. (Springer, 2009).
1449 74. Gu, Z., Eils, R. & Schlesner, M. Complex heatmaps reveal patterns and correlations in
1450 multidimensional genomic data. *Bioinformatics* **32**, 2847–2849 (2016).
1451 75. Robinson, A. E. *et al.* Lysine and Arginine Protein Post-translational Modifications by
1452 Enhanced DIA Libraries: Quantification in Murine Liver Disease. *J. Proteome Res.* **19**, 4163–
1453 4178 (2020).
1454 76. Berle, M. *et al.* Novel protein signatures suggest progression to muscular invasiveness in
1455 bladder cancer. *PloS One* **13**, e0206475 (2018).
1456 77. Parker, S. J., Venkatraman, V. & Van Eyk, J. E. Effect of peptide assay library size and
1457 composition in targeted data-independent acquisition-MS analyses. *Proteomics* **16**, 2221–
1458 2237 (2016).

1459 78. Parker, S. J. *et al.* Identification of a Set of Conserved Eukaryotic Internal Retention Time
1460 Standards for Data-independent Acquisition Mass Spectrometry. *Mol. Cell. Proteomics*
1461 *MCP* **14**, 2800–2813 (2015).
1462 79. Röst, H. L. *et al.* OpenSWATH enables automated, targeted analysis of data-independent
1463 acquisition MS data. *Nat. Biotechnol.* **32**, 219–223 (2014).
1464 80. Teleman, J. *et al.* DIANA--algorithmic improvements for analysis of data-independent
1465 acquisition MS data. *Bioinforma. Oxf. Engl.* **31**, 555–562 (2015).
1466 81. Röst, H. L. *et al.* TRIC: an automated alignment strategy for reproducible protein
1467 quantification in targeted proteomics. *Nat. Methods* **13**, 777–783 (2016).
1468 82. Choi, M. *et al.* MSstats: an R package for statistical analysis of quantitative mass
1469 spectrometry-based proteomic experiments. *Bioinforma. Oxf. Engl.* **30**, 2524–2526 (2014).
1470 83. Li, H. Aligning sequence reads, clone sequences and assembly contigs with BWA-MEM.
1471 *ArXiv13033997 Q-Bio* (2013).
1472 84. Faust, G. G. & Hall, I. M. SAMBLASTER: fast duplicate marking and structural variant read
1473 extraction. *Bioinforma. Oxf. Engl.* **30**, 2503–2505 (2014).
1474 85. Sherry, S. T. *et al.* dbSNP: the NCBI database of genetic variation. *Nucleic Acids Res.* **29**, 308–
1475 311 (2001).
1476 86. 1000 Genomes Project Consortium *et al.* A global reference for human genetic variation.
1477 *Nature* **526**, 68–74 (2015).
1478 87. Mills, R. E. *et al.* Natural genetic variation caused by small insertions and deletions in the
1479 human genome. *Genome Res.* **21**, 830–839 (2011).

1480 88. Li, H. *et al.* The Sequence Alignment/Map format and SAMtools. *Bioinformatics* **25**, 2078–
1481 2079 (2009).
1482 89. Okonechnikov, K., Conesa, A. & García-Alcalde, F. Qualimap 2: advanced multi-sample
1483 quality control for high-throughput sequencing data. *Bioinforma. Oxf. Engl.* **32**, 292–294
1484 (2016).
1485 90. *Picard toolkit*. *Broad Institute, GitHub repository* (Broad Institute, 2018).
1486 91. Benjamin, D. *et al.* Calling Somatic SNVs and Indels with Mutect2. *bioRxiv* 861054 (2019)
1487 doi:10.1101/861054.
1488 92. Wang, K., Li, M. & Hakonarson, H. ANNOVAR: functional annotation of genetic variants from
1489 high-throughput sequencing data. *Nucleic Acids Res.* **38**, e164–e164 (2010).
1490 93. Gehrke, S. *et al.* Red Blood Cell Metabolic Responses to Torpor and Arousal in the
1491 Hibernator Arctic Ground Squirrel. *J. Proteome Res.* **18**, 1827–1841 (2019).
1492 94. Nemkov, T., Reisz, J. A., Gehrke, S., Hansen, K. C. & D'Alessandro, A. High-Throughput
1493 Metabolomics: Isocratic and Gradient Mass Spectrometry-Based Methods. *Methods Mol.*
1494 *Biol. Clifton NJ* **1978**, 13–26 (2019).
1495 95. Nemkov, T., D'Alessandro, A. & Hansen, K. C. Three-minute method for amino acid analysis
1496 by UHPLC and high-resolution quadrupole orbitrap mass spectrometry. *Amino Acids* **47**,
1497 2345–2357 (2015).
1498 96. Huber, W., von Heydebreck, A., Sültmann, H., Poustka, A. & Vingron, M. Variance
1499 stabilization applied to microarray data calibration and to the quantification of differential
1500 expression. *Bioinforma. Oxf. Engl.* **18 Suppl 1**, S96-104 (2002).

1501 97. Agarwal, N. *et al.* GON4L Drives Cancer Growth through a YY1-Androgen Receptor-CD24
1502 Axis. *Cancer Res.* **76**, 5175–5185 (2016).
1503 98. Sanjana, N. E., Shalem, O. & Zhang, F. Improved vectors and genome-wide libraries for
1504 CRISPR screening. *Nat. Methods* **11**, 783–784 (2014).
1505 99. Imkeller, K., Ambrosi, G., Boutros, M. & Huber, W. gscreend: modelling asymmetric count
1506 ratios in CRISPR screens to decrease experiment size and improve phenotype detection.
1507 *Genome Biol.* **21**, 53 (2020).
1508 100. Joung, J. *et al.* Genome-scale CRISPR-Cas9 knockout and transcriptional activation
1509 screening. *Nat. Protoc.* **12**, 828–863 (2017).
1510 101. Winter, J. *et al.* caRpools: an R package for exploratory data analysis and documentation of
1511 pooled CRISPR/Cas9 screens. *Bioinforma. Oxf. Engl.* **32**, 632–634 (2016).
1512 102. Love, M. I., Huber, W. & Anders, S. Moderated estimation of fold change and dispersion
1513 for RNA-seq data with DESeq2. *Genome Biol.* **15**, 550 (2014).
1514 103. Bates, D., Mächler, M., Bolker, B. & Walker, S. Fitting Linear Mixed-Effects Models Using
1515 lme4. *J. Stat. Softw.* **67**, 1–48 (2015).
1516 104. Kuznetsova, A., Brockhoff, P. B. & Christensen, R. H. B. lmerTest Package: Tests in Linear
1517 Mixed Effects Models. *J. Stat. Softw.* **82**, 1–26 (2017).
1518 105. Cerami, E. *et al.* The cBio Cancer Genomics Portal: An Open Platform for Exploring
1519 Multidimensional Cancer Genomics Data. *Cancer Discov.* **2**, 401–404 (2012).
1520 106. Gao, J. *et al.* Integrative Analysis of Complex Cancer Genomics and Clinical Profiles Using
1521 the cBioPortal. *Sci. Signal.* **6**, pl1–pl1 (2013).

1522 107. Perez-Riverol, Y. *et al.* The PRIDE database and related tools and resources in 2019:
1523 improving support for quantification data. *Nucleic Acids Res.* **47**, D442–D450 (2019).
1524